THESIS

THE HYDROCLIMATE AND ENVIRONMENTAL RESPONSE TO WARMING IN THE SOUTHWESTERN US: A STUDY ACROSS THE MID-MIOCENE CLIMATE OPTIMUM

Submitted by

Siânin Spaur

Department of Geosciences

In partial fulfillment of the requirements

For the Degree of Master of Science

Colorado State University

Fort Collins, Colorado

Summer 2022

Master's Committee:

Advisor: Jeremy Caves Rugenstein

Joe Sertich
Jim Hurrell

ABSTRACT

THE HYDROCLIMATE AND ENVIRONMENTAL RESPONSE TO WARMING IN THE SOUTHWESTERN US: A STUDY ACROSS THE MID-MIOCENE CLIMATE OPTIMUM

Predictions for the effects of modern climate change on the southwestern US tend to suggest increased aridity, which is incompatible with paleoclimate data from other warm, high pCO_2 periods. The Mid-Miocene Climate Optimum (MMCO; ~17-14 Ma) represents a period of warm global temperatures and high pCO_2 similar to the projected pCO_2 for future decades. We present new stable isotope records of mid-Miocene terrestrial carbonates from the Española basin in northern NM, along with new $^{40}Ar/^{39}Ar$ ages that establish an updated, high resolution age model for the Miocene-aged basin sediments. Our $\delta^{18}O$ and $\delta^{13}C$ records span 17-12 Ma, recording the extent of the MMCO and the beginning of late Miocene cooling. We use $\delta^{18}O$ as a measure of the balance between summertime and wintertime precipitation and $\delta^{13}C$ as a reflection of soil productivity. We find evidence for an increasingly winter-wet climate in the southwest US during the MMCO; when compared to modern precipitation $\delta^{18}O$, the carbonate $\delta^{18}O$ record suggests that the region received more westerly-derived, wintertime precipitation than it does today. This indicates that El Niño Southern Oscillation (ENSO) was operating during the MMCO and may have even been stronger than today; it seems to have been particularly strong during cooler periods during the MMCO, suggesting that cooler temperatures and high pCO_2 may be favorable to ENSO. We also find that increases in wintertime precipitation are highly correlated with increases in soil productivity, suggesting that the amount of cool-season precipitation is a main control on vegetation for the region. Changes in the seasonal hydroclimate

and soil productivity agree well with the paleontological record at the site, which show a diverse and dynamic faunal assemblage that evolved with the hydroclimate. Collectively our data do not support increased aridity in the southwest US during warm, high pCO_2 periods, instead suggesting a shift towards increased cool-season precipitation that drives higher soil productivity, causing dynamic changes in the faunal and floral assemblage of the region.

ACKNOWLEDGEMENTS

First and foremost, I would like to thank my graduate advisor, Jeremy Caves Rugenstein, for his guidance, expertise, and optimism during this project. Without his support and character I would not have been able to pursue my goals towards a graduate degree, and certainly would not have had as much fun. I would like to thank my committee, Joe Sertich and Jim Hurrell, for their contributions to this project. I would also like to thank my collaborator Dan Koning for his invaluable knowledge of the Española basin, our field expeditions would not have been successful without him.

Funding and support from the Awards for Geochronology Student Research (AGeS) made this work possible and gave me the valuable opportunity to expand my knowledge and skillset. I would like to thank Matt Heizler for serving as my geochronology mentor and for dedicating so much time and effort to this project. I would also like to thank Jeff Knot and Nelia Dunbar for their work on the tephrachronological interpretations incorporated into this study.

I also thank Katie Snell for her willingness to collaborate; she provided valuable insights throughout my graduate experience and opened her lab up to me when our instrument would not work. I would also like to thank Gary Morgan and Garrett Williamson for their help in understanding the paleontology at Española, and Scott Aby for allowing us to turn his home into a water-sampling research center. I would also like to recognize that our area of study comprises ancestral lands of the Ute and Tiwa peoples and is now home to the Eight Northern Pueblos of New Mexico whose lands we have been fortunate to study; I thank Adam Duran from the Pueblo of Pojoaque for his willingness to work with us and allow us land access and Charles Goodluck from the Navajo Nation for his enthusiastic field assistance.

Finally, I would like to thank my friends, partner, and the fellow graduate students of the Geosciences department. Together you have created a supportive, thoughtful, and fun environment, and I am grateful to have shared this experience with you all.

TABLE OF CONTENTS

LIST OF TABLES

LIST OF FIGURES

Figure

Introduction

The combination of ongoing severe drought and projected population increase in the southwestern United States necessitates robust predictions of the future hydroclimate of the region. Model predictions of the annual precipitation (P) change range from mild decreases to no change in the western US (Seager and Vecchi, 2010; Schmidt and Grise, 2021; Simpson et al., 2021), but evapotranspiration (ET) is widely projected to increase as surface temperatures rise (Douville et al., 2021; Mankin et al., 2017) and as CO2 fertilization creates a "greener" southwest, driving an increase in transpiration (Mankin et al., 2017). Consequently, runoff (Q), defined as the difference between precipitation and evapotranspiration (Q = P – ET) is projected to decrease in the southwestern US (Overpeck and Udall 2020 (PNAS); Milly and Dunne 2020 (Science).

However, changes in P and, hence Q, in the southwestern US are difficult to constrain due to the hydroclimatology of the region. Cool-season precipitation is delivered by the westerly jet, which is strongly controlled by the El Niño Southern Oscillation (ENSO) and corresponding sea surface temperature (SST) changes in the tropical Pacific. How the tropical Pacific will respond to warming remains hotly debated, with theory and models both supportive of increases or decreases in the strength of the Walker Circulation (Vecchi et al. 2006 (Nature); Seager et al. 2019 (Nature Climate Change); Coats and Karnauskas 2017; Olonscheck et al., 2020; Seager et al., 2019). Further, warm-season precipitation is delivered by the North American Monsoon, which has been challenging to successfully represent in models due to the complex influence of regional geography and large-scale drivers, poorly constraining its predicted response to modern climate change (Pascale et al. 2017 (Nature Climate Change); Geil et al., 2013, Castro et al., 2012). The uncertainties associated with modelling the sources of both cool-season and warm-

season precipitation make projections of hydroclimate change in the US southwest remain highly uncertain.

Predictions of increasing aridity in the southwestern US under elevated pCO_2 are inconsistent with geologic data from the mid-Pliocene Warm Period (mPWP; pCO_2 = 350-450 p.p.m. [Haywood et al., 2016]), which indicate wetter conditions in the western US: abundant lacustrine deposits suggest precipitation outpaced ET (Ibarra et al., 2018), terrestrial carbonates indicate strong ENSO conditions delivering wintertime moisture (Winnick et al., 2013), and climate models forced with Pliocene SST reconstructions show wetter subtropics (Burls and Federov, 2017). The disagreement between models and paleoclimate data necessitates the study of other high pCO_2, warm global climate events to further inform our understanding of the possible hydroclimate response. One such event is the Mid-Miocene Climate Optimum (MMCO; ~17-14 Ma), which was characterized by global temperatures 7-8°5 C warmer than preindustrial and atmospheric CO2 estimates of ~400-800 ppm (Steinthorsdottir et al., 2021; Guillermic et al., 2022), similar to end-of-century estimates of atmospheric CO2 and warming under extreme scenarios. Continental positions and topography were similar to modern, especially in North America (Mix et al. 2011; Chamberlain et al. 2012); the main notable difference was the existence of the Panama seaway during the middle Miocene (Haug et al., 2001), though it is unclear whether this caused large changes in North American climate (Federov et al., 2013; Zhang et al., 2012; Lunt et al., 2008). Although the MMCO is well established in the benthic paleoclimate record, continuous terrestrial records of the event are relatively scarce. Clumped isotope records, fossil plants and fossil tooth enamel show that the western US (the area west of and including the Rocky Mountains) experienced much higher mean annual temperatures during the MMCO (Methner et al., 2021; Mix and Chamberlain, 2014; Axelrod and Bailey, 1976;

Harris, 2016), and paleobotany data supports the existence of expansive warm-temperate evergreen broadleaf and mixed forests, woodlands, and shrublands that became increasingly fragmented during the Late Miocene (Pound et al., 2012). The existence of wooded environments in areas of modern desert suggest the possibility of wetter conditions than today and do not show support for increased aridity. The paleobotany records also find fairly large differences in climatic stability between different regions of the western US, emphasizing the importance of regional-scale climatic responses (Harris, 2016; Pound et al., 2012).

We present new authigenic carbonate $\delta^{18}O$ and $\delta^{13}C$ records from the Española Basin in northern NM that span the Miocene Climatic Optimum with an updated, high-resolution age model that incorporates newly dated tephra units. We use $\delta^{18}O$ to interpret changes in the seasonal hydroclimate regime, taking advantage of the large difference in $\delta^{18}O$ values between summertime and wintertime precipitation to the region (Tulley-Cordova et al., 2021). Thus our $\delta^{18}O$ record is not an indicator of wetness, but rather of changes in the balance between cool and warm season precipitation. In turn, pedogenic carbonate $\delta^{13}C$ reflects the amount of C sourced from atmospheric CO2 versus soil CO2 and is thus used as a proxy for primary productivity (Cerling, 1984; Quade, 1993; Caves et al. 2016). This provides a valuable understanding of regional plant productivity that can then be supplemented with fossil data, reflecting the influence of hydroclimate and CO2 fertilization (Rugenstein and Chamberlain 2018). The fluvial basin floor, wide alluvial slope, and proximity to high mountains that characterized the Española basin during the middle Miocene made it an ideal environment for a wide variety of flora and fauna (Aby et al., 2011). Mid-Miocene fossils in the basin have been the focus of paleontological studies for 150 years (Cope, 1877; Frick, 1926; Morgan, 2015), yielding a well-described faunal fossil record that indicates a rich and varied paleoenvironment completely different to that of the

region today (Aby et al., 2011; Kues and Lucas, 1979; Tedford and Barghoorn 1997). The fossil record spans the entirety of the MMCO and the subsequent transition to the cool climate of the late Miocene (Tedford, 1981), making it a valuable comparison to our new stable isotope record. We find evidence for a change in the seasonal balance of precipitation, causing changes in soil productivity and faunal assemblages in the area. Together these records shed light on the specific hydroclimate response of the southwestern US to a warmer world and the subsequent effects on vegetation and ecosystems as a whole.

Geologic Background

We focus on sediments exposed within the Española basin (Figure 1, 2), a large, 30 km wide rift basin located within the central Rio Grande Rift in north-central New Mexico near the towns of Española and Chimayo. The basin is bounded to the east by the Sangre de Cristo mountains and to the west by a complicated system of large displacement normal faults known as the Embudo-Santa Clara-Pajarito fault system (Koning et al. 2013). The large-scale tectonic evolution of the Rio Grande Rift created the Española Basin and caused significant faulting and downwarping of the basin floor beginning in the late Oligocene, followed by rifting and faulting of basin-fill sediments. The eastern part of the basin (of interest to this study) is a west-tilting half-graben, with strata dipping ~2-15° towards the major fault system that forms the western boundary of the basin. There are also numerous north-south striking normal faults within the basin, showing evidence for continuous low vertical displacement throughout rifting (Koning et al. 2013).

The Española basin serves as the type area for the Oligocene-Pleistocene Santa Fe Group, the siliciclastic and volcanic basin fill of the Rio Grande Rift. This Group consists primarily of basin-floor and basin-margin sediments deposited synchronously during rifting. The Sangre de

Cristo mountains served as a major source of sediment and water, allowing relatively fast and continuous sedimentation with many stream channels (Koning et al., 2005). These strata are divided into the older Tesuque Fm and younger Chamita Fm; in the eastern Española basin the former is divided into the Nambé, Skull Ridge, and Pojoaque members, and the latter is divided into the Hernandez, Vallito, Cejita, and Cuarteles Mbrs (from oldest to youngest; Galusha and Blick, 1971). A magnetostratigraphic study (Barghoorn, 1981) identified a potential unconformity at the Pojoaque-Skull Ridge contact, but Koning et al. (2005) notes that the contact appears gradational in some areas making the existence of an unconformity unclear. Santa Fe Group strata generally coarsen upwards; Tesuque Fm sediments are mostly very fine-medium sandstones with minor conglomeratic channel deposits, while the Chamita Fm has more abundant coarse channel deposits. The geologic sections sampled in this study include the three members of the Tesuque Fm and the Cuarteles Mbr of the Chamita Fm, which collectively provide a continuous geologic record across the middle Miocene (Figure 2). The Tesuque Fm contains abundant pedogenic carbonates, mainly as nodules, rhizoliths, and BK-horizons in paleosol facies. Carbonate cemented sandstones, likely cemented by groundwater, are also abundant throughout the section. The Cuarteles Mbr does not have abundant carbonate, resulting in sparser sampling of this unit. Throughout this sedimentary sequence, there are abundant tephra layers, with fifty ash units identified in the sections used for this study. Tephrachronologic analysis has identified the southern Nevada volcanic field and the Snake River Plain-Yellowstone hot spot track as the major source regions of Miocene ashes in the Española basin (Slate et al., 2013).

Climatic Background

The difficulties of predicting climate changes in the US southwest lie in the complicated hydroclimate regime of the region. Its location between mid-latitude and subtropical atmospheric circulation systems introduces a high degree of climatic variability (Sheppard et al., 2002). Regional hydroclimate is affected by two independent sources of moisture: wintertime precipitation sourced from the Pacific Ocean, and summertime precipitation from the North American Monsoon (NAM) (Sheppard et al., 2002). During positive ENSO phases, warm eastern equatorial Pacific sea surface temperatures (SST) create wetter conditions in the southwest during the winter and spring (McPhaden et al., 2006). Conversely, during La Niña conditions, cool eastern Pacific SST cause drier winters (McPhaden et al., 2006). This wintertime precipitation can also be affected by the Pacific Decadal Oscillation (PDO) – the long-term pattern of northern Pacific SST variability – which shifts the latitudinal position of the northern hemisphere jet stream, affecting the amount of precipitation delivered to the southwest (Zhang et al. 1997). ENSO and PDO can either amplify or interfere with each other, creating additional variability in wintertime precipitation in the southwest (Sheppard et al., 2002). NAM delivers up to 50% of annual rainfall to New Mexico (Sheppard et al., 2002), mainly sourcing moisture from the Gulf of California, Gulf of Mexico, and Mexico. Terrestrial evapotranspiration over Mexico and Central America plays as large a role as oceanic evaporation, contributing up to ~40% of monsoonal moisture (Hu & Dominguez, 2015). Both the variety of NAM moisture sources and the effect of the midtropospheric subtropical ridge create high spatial and temporal monsoonal variability. The seasonality of precipitation sources in the southwest leads to a seasonality in precipitation $\delta^{18}O$: westerly Pacific moisture is characterized by a relatively low $\delta^{18}O$ (-15 to -10 ‰), while NAM precipitation has a relatively high $\delta^{18}O$ (-10 to 0 ‰; Tulley-

Cordova et al., 2021) due to the high composition of evapotranspired moisture (Hu & Dominguez, 2015). The ~10‰ difference between ENSO-derived precipitation and NAM precipitation allows $\delta^{18}O$ to be a useful tracer when examining changes in the relative contribution of each source to the hydroclimate of the Southwest.

Methods

Field Methods

We sampled carbonates from six stratigraphic sections in the eastern Española basin, following transects established by Barghoorn (1981) in order to tie our samples to the magnetostratigraphy detailed in that study. Of these, the West Arroyo Seco Hanging Wall, La Puebla, and Cuarteles sections have been re-described in detail by Koning et al. (2013). We re-measured and described in greater detail the Nambé, Arroyo de los Martinez, and Pojoaque sections from Barghoorn (1981) using an Abney level and Jacob staff. We sampled the upper part of the lowermost member, Nambé, which is characterized by pinkish sand, silt, and clay-filled sand with occasional conglomerate lenses and the Nambé white ash zone. The West Arroyo Seco Hanging Wall, La Puebla, and Arroyo de los Martinez sections comprise the Skull Ridge Mbr and the lower Pojoaque Mbr. These sections are dominated by very fine to medium grained sandstones and silty sandstones with sparse conglomeratic channel deposits, many ash beds comprising the Skull Ridge ash zone, and the highest abundance of carbonates seen in the sections sampled. The Pojoaque section is the type section of the Pojoaque member, with salmon-colored silty sands slightly coarser than those in the Skull Ridge Mbr, minor pebbly channel deposits, and ash beds comprising the Pojoaque white ash zone. The uppermost Cuarteles section is the coarsest grained section with frequent gravelly conglomerate layers; sparse sampling in this section reflects a lack of carbonate in the Cuarteles Mbr.

The general abundance of carbonates in these sections allowed for sampling of a variety of carbonate sample types (Figure 3). Pedogenic carbonates sampled include nodules, rhizoliths (root casts), and cemented soil BK-horizons (n=3), all of which are thought to have formed in the vadose zone of a paleosol. We also sampled ledge-forming carbonate-cemented sandstones

(referred to as cements in this study), with cementation thought to have occurred by shallow groundwater flow after deposition (Cavazza 1986; Spötl and Wright, 1992). Our final sample category includes weakly cemented sandstone, siltstone, or conglomerate bulk samples with enough carbonate cement matrix to react with HCl, which we refer to as matrix samples. All sample types are consistently found throughout all sections (Figure 4), although nodules in the upper half of the compiled section appear more immature than those in the lower half, and the Cuarteles section lacks carbonate in general. Modern water samples from groundwater and streams in the area were also collected in the fall and spring for stable isotope analysis in order to compare their values to those of the Miocene-aged carbonates. Shallow groundwater used for drinking was sampled throughout a year-long period to produce a complete time series. Stream water samples were collected in October and May. All water samples were filtered upon collection using 0.23 um filters and stored in 2 mL Fisher autosampler vials. All water samples were immediately wrapped in parafilm to prevent atmospheric exchange and stored at ~40°F for one month until analysis.

Geochronology

We establish a geochronology based upon two independent methods: (1) the previous magnetostratigraphy work by Barghoorn (1981), and; (2) new $^{40}Ar/^{39}Ar$ dates of many of the major Miocene ashes present in the basin. These ash units have yielded $^{40}Ar/^{39}Ar$ and fission-track ages in past studies (Izett and Obradovich, 2000; McIntosh and Quade, 1995; Izett and Naeser, 2000), but the technological advances of geochronological instruments allowed for re-dating of these ashes with increased precision. We sampled all ash beds that appeared unaltered (based upon color in the field; n = 42), specifically sampling the base of each ash unit where the

presence of crystals is most likely. All ash samples were screened for the presence of sanidine for $^{40}Ar/^{39}Ar$ dating, yielding nine dateable samples. Of these, two units were dated using samples collected outside of the study area due to a lack of dateable material in the samples we collected. The samples used for analysis were confirmed to be the same units as those that we sampled through tephrachronological analysis.

Cemented ash samples were crushed, and all ash samples were sieved to separate the 60-100 mesh material of interest. The K-feldspar portion of each sample was concentrated using heavy liquid separation and sanidine crystals were handpicked under a polarizing transmitted light microscope. Crystals were irradiated in three irradiations and then fused using a CO_2 laser. All samples were analyzed using an ARGUS VI multi-collector mass spectrometer with one electron multiplier (CDD) (Appendix C).

Analysis

All carbonate samples were powdered by hand with either a Dremel or a mortar and pestle. Depending on carbonate content, 220-350 ug of powdered sample were weighed and placed in 12 ml Exetainer vials, which were flushed with helium and then reacted with phosphoric acid. Carbonate samples analyzed at the University of Wyoming Stable Isotope Facility were reacted with 99.99% phosphoric acid for 24 hours and analyzed for $\delta^{18}O$ and $\delta^{13}C$ using a Thermo Delta V continuous-flow stable isotope ratio mass spectrometer attached to a Thermo Gasbench yielding a standard uncertainty < 0.5‰. Carbonate samples measured at the University of Colorado Boulder Earth Systems Stable Isotope Lab were reacted with 105% orthophosphoric acid for 1 hour and analyzed using a Thermo Delta V attached to a Thermo Gasbench II with precision within 0.1‰. Modern water samples were analyzed for $\delta^{18}O$ and δD at Colorado State

University EcoCore Analytical Facility on an L-2130 Picarro Water Isotope Analyzer. Details about stable isotope anaylsis can be found in Appendix B.

Results

Geochronology

Ages for nine ash units in the Española basin were obtained using $^{40}Ar/^{39}Ar$ dating (Table 1). Previous magnetostratigraphic work along these sections (Barghoorn 1981) was additionally used to inform the applied age model. The La Puebla section included only one dateable ash, so the C5ADr-C5aDn magnetic reversal was used to calculate a sedimentation rate and aid in correlating the section to the Arroyo de los Martinez section. The magnetic data was also used to establish the plausibility of the 40Ar/39Ar ages; ages determined for four additional tephra layers were not included in the study because they strongly disagreed with the age ranges indicated by the magnetostratigraphy as well as biostratigraphy developed from adjacent fossil sites. These four samples lacked juvenile grains, yielding anomalously old ages from inherited grains that may be thought of as maximum depositional ages. White Ashes No. 2 and 3 yielded ages that were slightly too old to agree with the magnetostratigraphic record, but each had a sub-population of younger individual crystal ages indicating an age that does agree with the magnetostratigraphy. These alternate ages were considered instead of the ages indicated by the main populations of single crystal ages in light of the magnetostratigraphic constraints. The alternate $^{40}Ar/^{39}Ar$ age of White Ash No. 2 (16.02 ± 0.12 Ma) is still slightly too old to agree with the magnetostratigraphy, so we use an age of 15.9 Ma for this ash because it agrees with the magnetostratigraphic data and falls within the error associated with the analysis. White Ash No. 3 was able to be redated with more material, and this yielded a new age in close agreement with the alternate age indicated by the younger sub-population of grains in the first analysis. The ages associated with the most recent Geomagnetic Polarity Time Scale (Ogg 2020) were used when

considering the magnetostratigraphic data. Thus, we present new, revised ages for five previously dated ash units and four ages of previously undated ashes.

$\delta^{18}O$ Results

The $\delta^{18}O$ values for Española carbonates range from -18‰ to -6.5‰ (Figure 5). When compared to the benthic $\delta^{18}O$ record (DeVleeschouwer et al., 2017), the carbonates show a slight decrease in $\delta^{18}O$ throughout the MMCO and a large increase in $\delta^{18}O$ following the climate event. Local maxima and minima occur throughout the record; notably, there are two periods of low $\delta^{18}O$ coinciding with cool events represented in the benthic record (13.9-14.3 Ma and 15.2-15.9 Ma).

The $\delta^{18}O$ values recorded by groundwater carbonates versus soil water carbonates reveals an offset between the two records, with the groundwater carbonates showing lower $\delta^{18}O$ than the soil water carbonates (Figure 5). There are only three events during the MMCO in which the two datasets converge on the same values; two of those events occur during the cool periods shown in the benthic record. Comparison of $\delta^{18}O$ vs $\delta^{13}C$ by sample type (Figure 6) reveals very similar relationships for all types. An ANOVA test ($\alpha = 0.05$) and pairwise comparison using estimated marginal means of the $\delta^{18}O$ data by sample type reveals two groups of statistically similar values: *(1)* rhizoliths, cements, and matrix samples, and *(2)* matrix and nodules (Tables B, C; Figure 7).

$\delta^{13}C$ Results

The $\delta^{13}C$ values for Española carbonates range from -8.2‰ to -3‰ (Figure 5). There is a slight decrease in $\delta^{13}C$ throughout the record, although this trend is observed to lag the benthic extent

of the MMCO in a similar manner to the $\delta^{18}O$ record. The $\delta^{13}C$ data show dramatic swings that are highly correlated with the $\delta^{18}O$ record, indicating linked drivers of change for the two datasets. Minima in the $\delta^{13}C$ record occur concurrently with minima in the $\delta^{18}O$ data and cool periods in the benthic record. An ANOVA test ($\alpha = 0.05$) of the $\delta^{13}C$ data by sample type showed two groups with statistical similarities: *(1)* rhizoliths and cements, and *(2)* cements, nodules, and matrix (Tables D, E).

Modern Water $\delta^{18}O$ Results

Precipitation $\delta^{18}O$ measured by Tulley-Cordova et. al (2021) in the Four Corners region (~400 km west of Española) shows values from -15‰ to -5‰, with a noticeable increase in $\delta^{18}O$ during June-August (Figure 8). A groundwater $\delta^{18}O$ time series collected in Ojo Sarco, NM, (~32 km northeast of Española and ~600 m higher in elevation) displays extremely low temporal variability with consistent values around -12.5‰ throughout the year. Nearby Sarco Creek shows a similar trend to the groundwater, with little temporal variability and similar $\delta^{18}O$ values averaging -12‰. To characterize the $\delta^{18}O$ of modern waters in the larger region surrounding the Española basin, stream samples were collected from southern CO and northern NM at a range of elevations, including areas along the Sangre de Cristo and Jemez mountains. Due to the variability in location and elevation of these samples, the stream $\delta^{18}O$ values have an almost 5‰ range with an average of -13.14‰ ± 1.27‰.

Discussion

Our new stable isotope paleoclimate record combined with the updated ash geochronology provide a high-resolution record of environmental change in the Española basin across the MMCO. We find that shifts in seasonal precipitation are highly correlated with changes in soil productivity, causing dynamic shifts in faunal assemblage and the ecosystem as a whole. First, we discuss the new $^{40}Ar/^{39}Ar$ ages of Española basin ashes and their implications for the member ages and biostratigraphy of the Tesuque Formation in which our carbonate stable isotope record is hosted. Second, we consider the $\delta^{18}O$ of modern and past precipitation and examine changes in Española $\delta^{18}O$ during the MMCO, discussing possible drivers of change. We consider possible factors that affect the $\delta^{13}C$ record and discuss the environmental implications of the data by comparing it to the extensive and diverse paleontological record at the site. Lastly, we identify the larger trends indicated by our paleoclimate record and consider them in the context of modern climate change.

Revised Tesuque Formation Member Ages

The age model applied to our record indicates that our paleoclimate record spans 12.01-17.65 Ma, making it one of the best-dated mid-Miocene terrestrial paleoclimate records in the world. The end of the MMCO in the benthic record correlates well to a positive shift in Española $\delta^{18}O$ that we interpret as the end of the MMCO in our record, indicating good agreement between the age model of the benthic record (DeVleeschouwer et al., 2017) and our independently dated record. Almost all of the new $^{40}Ar/^{39}Ar$ ages of previously dated ashes indicate older ages than the previous analyses (Table 1; Izett & Obradovich, 2000; Izett & Naeser, 1981; McIntosh & Quade, 1995). Our new age model indicates the following ages for the members of the Tesuque

Fm: 16.25-15.13 Ma, Skull Ridge Mbr; 15.13-13.4 Ma, Pojoaque Mbr (Appendix A). The Nambé section used for this study does not include the lower Nambé Mbr, so only an upper age boundary for the Nambé (16.25 Ma) can be determined. The age of the Skull Ridge-Pojoaque contact does not agree with the paleomagnetic record (disagree by ~400kyr; Barghoorn, 1981). However, there is an unconformity at this contact that complicates interpretations of the paleomagnetic record, and the coarse sampling resolution of the past study (Barghoorn, 1981) may have caused some magnetic reversals to be missed, possibly explaining the disagreement between the ages indicated by the magnetostratigraphy and our age model. The updated ages of the members are similar to past estimates using previous dating of ash units (Koning et al., 2013) and biostratigraphy (Tedford, 1981), although our age model indicates that the Skull Ridge has a shorter temporal extent than previously thought. In relation to the North American land mammal ages (NALMA), our age model places the Nambé Mbr in the Hemingfordian, the Skull Ridge in the late Hemingfordian and early Barstovian, and the Pojoaque in the latter half of the Barstovian, ending in the early Clarendonian.

Modern Water $\delta^{18}O$

The annual precipitation $\delta^{18}O$ from Tulley-Cordova et al. (2021; Figure 8) indicates an almost 10‰ difference between wintertime and summertime precipitation. Cool-season precipitation consistently has a relatively low $\delta^{18}O$, rarely being higher than -10ee; this part of the annual cycle reflects precipitation delivered by the westerlies from the Pacific Ocean, which is relatively depleted in ^{18}O by the time it falls in New Mexico. In the summertime, specifically June-August, precipitation $\delta^{18}O$ is at a maximum, with values as high as -1‰ and an average of -5‰. These values reflect the introduction of NAM precipitation from the south which is much less depleted

in ^{18}O compared to the westerly moisture, causing it to have a relatively high $\delta^{18}O$. Groundwater and stream water display little annual variability, indicating that these reservoirs are likely being recharged by the same seasonal water source; if they were continually recharged throughout the year they would mirror the precipitation $\delta^{18}O$ signal, but instead they maintain one $\delta^{18}O$ value that likely reflects the precipitation $\delta^{18}O$ of the months/season during which it is replenished. During ENSO years the amount of westerly precipitation to the region increases, which would lower the average annual $\delta^{18}O$ as the system would receive more low $\delta^{18}O$ precipitation than usual. On the other hand, if the ENSO system were to weaken and the region received very little westerly precipitation on a long time scale, average annual precipitation $\delta^{18}O$ would increase as high $\delta^{18}O$, NAM precipitation dominated the hydroclimate. This is the interpretive framework that we apply to our carbonate stable isotope records.

To compare the $\delta^{18}O$ of modern precipitation to Española carbonate $\delta^{18}O$ from the middle Miocene, we convert the average precipitation $\delta^{18}O$ to its equivalent carbonate value using the methodology of Kim and O'Neil (1997) and a temperature of formation 7°C warmer than modern, in consideration of MMCO temperature estimates (Steinthorsdottir et al., 2021). Since pedogenic carbonates are known to have a warm-season formation bias (Breecker et al., 2009), we calculate one value that represents a warm-season formation scenario (T=28°C), and one that considers mean annual temperature (T=19°C). The average $\delta^{18}O$ of modern precipitation converted into its equivalent carbonate values under formation regimes in warm-season temperatures and annually averaged temperatures are -7.60‰ and -10.26‰, respectively (Figure 5). These values are within the measured $\delta^{18}O$ range of Española carbonates, although the majority of Española $\delta^{18}O$ data is more negative.

Hydroclimate Changes Indicated by $\delta^{18}O$

The variety of carbonate sample types used in this study may suggest that the large swings observed in the $\delta^{18}O$ record reflect differences between sample types. Although the statistical analysis did find some differences between means, it is important to note that all sample type means fall within a 1‰ range (Figure 7). Additionally, the statistical analysis (Table 2, 3) showed that, when grouped by statistical similarity, the two groups overlap with each other, indicating a degree of relatedness between all sample types. It is difficult to address possible formation differences between sample types because the formation conditions of different kinds of terrestrial carbonates are not well understood. The water source for Española basin carbonates may vary between groundwater vs soil water, and the timing of formation may impart a bias towards, for example, summertime waters (Breecker et al., 2009). We also assume that all sampled carbonates formed under equilibrium formation, allowing us to use equilibrium fractionation factors. Although differences in these formation conditions could influence trends in the $\delta^{18}O$ record, the impressive correlation of our $\delta^{13}C$ record to our $\delta^{18}O$ record does provide support that Española $\delta^{18}O$ does reflect environmental changes, since the oxygen and carbon are sourced from different pools and thus are independent records. Comparing $\delta^{18}O$ to $\delta^{13}C$ by sample type also reveals very similar relationships for all types, which suggests similar conditions of formation for all sample types (Figure 6). Although we believe the changes in the isotope records reflect environmental signals, we cannot discern whether they reflect seasonal or interannual variability because of the time-averaged nature of carbonate formation.

Española $\delta^{18}O$ values decrease across the MMCO by about 2‰, which we interpret as a shift in the seasonal precipitation balance towards the cool-season, westerly precipitation. This could reflect two scenarios: (1) westerly precipitation did not change but NAM precipitation decreased,

or (2) NAM precipitation did not change and westerly precipitation increased. Paleobotanical and paleontological studies indicate rich floral and faunal assemblages in the western US that would have required wetter conditions than exist in those regions today (Pound et al., 2012; Steinthorsdottir et al., 2021), making the drying indicated in the first scenario unlikely. Additionally, our comparison of modern water $\delta^{18}O$ values to mid-Miocene carbonate $\delta^{18}O$ shows that the Española carbonates generally show lower $\delta^{18}O$ than they would if the seasonal precipitation balance was the same as the modern (Figure 5); when both warm-season and annually-averaged carbonate formation scenarios are considered, both yield $\delta^{18}O$ values higher than the majority of the paleoclimate $\delta^{18}O$ data. This difference between the paleoclimate and modern $\delta^{18}O$ suggests that the region received more wintertime precipitation during the MMCO than it does today. The comparison of groundwater and soil water carbonate $\delta^{18}O$ (Figure 5) additionally supports this interpretation; the only periods in which groundwater and soil water $\delta^{18}O$ overlap during the MMCO (15.5-15.7 Ma; 13.9-14.3 Ma) coincide with minima in the $\delta^{18}O$ record that we interpret as peaks in cool-season precipitation. Groundwater $\delta^{18}O$ is negatively offset from soil water $\delta^{18}O$ due to most groundwater replenishment being sourced from the low $\delta^{18}O$ wintertime precipitation while summertime NAM precipitation evaporates too quickly to be incorporated (Tulley-Cordova et al., 2021). Thus the overlapping $\delta^{18}O$ values of groundwater and soil water likely reflect an increased connectivity between the two reservoirs resulting from an overall increase of water in the system and minimal evaporative effects affecting soil water; this suggests an increase in precipitation during cool seasons when evaporative effects are low, consistent with our interpretation of increased wintertime precipitation. Together, these lines of evidence suggest that the decrease in Española $\delta^{18}O$ across the MMCO is attributable to a shift in the seasonal precipitation balance towards a more winter-wet environment; whether the activity

of NAM changed throughout this time is unclear, although the abundance of carbonates throughout the section does indicate the activity of continuous wet-dry cycles that may point to dry summers (Breecker et al., 2009).

The similarity of converted modern water $\delta^{18}O$ values to mid-Miocene $\delta^{18}O$ indicates that the regional paleoprecipitation regime was not dramatically different from today, with both ENSO and NAM operating during this time. Although the activity of NAM in the past is poorly understood, there is evidence for an active, if not stronger, ENSO system during the middle to late Miocene. Model simulations with high pCO_2 and middle-Miocene topography (Krapp and Jungclaus, 2015) show enhanced Pacific variability favoring strong ENSO conditions, and evidence of ENSO activity in the geologic record during the late Miocene additionally supports the idea that the system operated during the Miocene in a similar manner to modern (Galeotti et al., 2010). The reduced meridional temperature gradient of the MMCO (Goldner et al., 2014) has been suggested to have extended ENSO teleconnections (Galeotti et al., 2010) and would have caused decreased poleward heat transport that may have resulted in a more energetic ENSO system (Krapp and Jungclaus, 2015). These mechanisms supporting a stronger ENSO system during the MMCO are possible explanations for the increase in cool-season ENSO precipitation we observe in the Española $\delta^{18}O$ record. Local minima in the Española $\delta^{18}O$ record also coincide with cool periods represented in the benthic record, suggesting that these local periods of cooling within the MMCO were associated with stronger ENSO activity, although the mechanisms behind this are unclear.

Productivity changes indicated by $\delta^{13}C$

All mean sample type $\delta^{13}C$ values fall within a 0.5‰ range, and when grouped by statistical

similarity both groups overlap, indicating a degree of similarity between carbonate sample type $\delta^{13}C$. Although carbonate $\delta^{13}C$ may be affected by carbonate formation conditions like timing of formation and whether there are equilibrium conditions, $\delta^{13}C$ does not reflect changes in water source like $\delta^{18}O$ does. Instead, terrestrial carbonate $\delta^{13}C$ is commonly interpreted as reflecting some balance between atmospheric CO_2 and soil CO_2, the two possible sources of carbon during formation (Cerling, 1984; Quade, 1993; Caves et al. 2016). Thus $\delta^{13}C$ can be used to reflect atmospheric pCO_2, however a comparison of our $\delta^{13}C$ record to a record of past pCO_2 (Guillermic et al., 2022) shows no correlation between the two records. It is also important to note that records of mid-Miocene pCO_2 are not continuous with little available data from ~14-15.5 Ma, making it difficult to compare to our high-resolution record. Since there is no discernable correlation between Española basin $\delta^{13}C$ and estimates of past pCO_2, we do not consider Española $\delta^{13}C$ to reflect atmospheric CO_2 concentrations. Records of $\delta^{13}C$ are also commonly used to reflect the proportion of C3 vs. C4 plants (O'Leary, 1988; Farquhar et al., 1989). However C4 grasses are not considered to have emerged until the late Miocene, about 6 Myr later (Edwards et al., 2010; Kohn and Fremd, 2008) and a stable isotope study of fossil teeth in the Española basin yielded no evidence supporting the existence of C4 plants during the time period included in this study (Magallanes, 2019). Thus, we interpret our $\delta^{13}C$ record as an indicator of soil productivity, where decreases in $\delta^{13}C$ indicate an increased availability of soil CO_2 as a source of carbon for carbonate formation, implying higher soil respiration rates and increased soil productivity. We apply this framework to our $\delta^{13}C$ record and interpret changes as reflecting soil productivity.

The $\delta^{13}C$ record shows a slight decrease across the MMCO, but the large swings throughout the record suggest that the region experienced relatively short-term and frequent changes in

productivity that were more important than a linear response to MMCO conditions. These changes reflect seasonal or interannual cycles of a dynamic ecosystem capable of supporting different levels of soil productivity and vegetation. A driver of this dynamic productivity is evidenced in the remarkable correlation between $\delta^{18}O$ and $\delta^{13}C$, where shifts towards more winter-wet conditions are associated with increases in soil productivity. This seems to be a significant control on productivity; every single period of increased productivity is associated with a concurrent increase in wintertime precipitation. This suggests that the amount of cool-season precipitation was the main control on soil productivity and vegetation in the southwest US during the Miocene. The link between winter moisture and vegetation in the western US has been found in modern studies of the region (Knowles et al., 2018; Scott et al., 2000; Tang et al., 2015) and during the Cenozoic in general (Kukla et al., 2022), where wintertime aridity has a larger impact than summer aridity on vegetation structure and increases in wintertime precipitation drive increases in biomass and shifts towards more wooded habitats. The balance between winter precipitation and summer evaporative demand is highly correlated with gross primary productivity in the western US; runoff (P-E) is largely only positive during cool seasons, making the cool-season precipitation the main source of water available for plant use (Hu et al., 2010; Knowles et al., 2018). The strong correlation between the independent $\delta^{13}C$ and $\delta^{18}O$ Española records suggests that the amount of cool-season precipitation was the main control on productivity and ecosystem structure in the southwest US during the middle Miocene.

Comparison of paleoclimate data to paleontological record

The paleontological record of the Española basin provides valuable insights into our interpretations of the regional paleoclimate. During the middle Miocene the Española basin

would have comprised a low-lying area adjacent to an alluvial slope at the foot of the Sangre de Cristo mountains, with many meandering streams incising the basin floor. This led to a mixed environment of savannas and forests, with more wooded areas occurring along streams and on the higher elevations of the alluvial fan (Kues and Lucas, 1979). Fossil plants (Axelrod and Bailey, 1979), petrified wood, and root casts with sizes ranging from those of small bushes to those of large trees indicate extensive and diverse flora. As the $\delta^{13}C$ record suggests, a dynamic ecosystem is indicated by the faunal fossil record; the faunal assemblages change throughout the MMCO in agreement with our isotope records. Stratigraphic constraints on historic fossil localities are poor, so observations about the fossil record can only be made by geologic member. The Nambé Mbr comprises the oldest portion of our paleoclimate record and has the sparsest fossil record, with the most abundant and diverse of the mammals found being ungulates (*Artiodactyla*) like camels (Morgan, 2015).

Fauna of the Skull Ridge Mbr are very diverse and represent a much more varied ecosystem than those of the Nambé; many new taxa appear in the Skull Ridge, including newly evolved species adapted for specific roles in the regional ecosystem (Tedford and Barghoorn, 1997). A *Sabal* palm fossil indicates a climate 7°C warmer than modern and a seasonal temperature range ~5°C less than today (Axelrod and Bailey, 1979), consistent with temperature estimates of the MMCO. Española fauna flourished during this period, including the highest diversity and abundance of camels in the record, horses, rhinos, deer, antelope, and carnivores including canids, felids, and primitive bears (Morgan, 2015). The appearance of abundant large herbivores including the browsing horse *Anchitherium* (Tedford and Barghoorn, 1997) and the long-necked camel *Aepycamelus* (Barghoorn 1985) indicate the presence of tall trees; the simultaneous appearance and continued survival of the high-crowned stenomyline camels indicate an availability of tough,

dusty grasses that would have comprised their diet. The introduction of mud turtles (Williamson et al., 2016) and a semiaquatic rhino reminiscent of a primitive hippo (*Teleoceras*; Morgan, 2015) also suggest more mesic conditions during this period. These faunas paint a picture of a rich environment capable of supporting a much wider range of vegetation than today, reflective of high pCO_2, warmer, and likely wetter conditions. Notably, the Skull Ridge Mbr completely encompasses a long period of increased wintertime moisture present in the $\delta^{18}O$ record that coincides with a significant peak in soil productivity at ~15.5 Ma. A more winter-wet hydroclimate regime would encourage the growth of larger vegetation and generally support higher primary productivity (Kukla et al., 2022), which is reflected in both the $\delta^{13}C$ and faunal records. The abundance of high-crowned, arid-adapted grazers suggests possible summer aridity, with larger vegetation being sustained either by stream water or groundwater replenished during the winter. The $\delta^{13}C$ record also does not indicate consistently high productivity throughout the duration of Skull Ridge deposition, so the mixed faunal record may also be reflecting changes in productivity on longer timescales than seasonal change.

The fossil record in the lower-middle Pojoaque Mbr is similar to the assemblage in the Skull Ridge, although some of the more specifically-adapted oreodonts disappear and many new faunas are introduced, including the first occurrence of the elephant-like gomphotheres in Española (Tedford 1981). Fossils in this portion of the Pojoaque are considered to reflect slightly drier conditions than the Skull Ridge, although the diverse faunal record of the Pojoaque Mbr overall reflects a variety of environmental conditions with changing faunal assemblages. The middle-upper Pojoaque includes gastropods, frogs, toads, salamanders (Aby et al., 2011), clam shells (McKinney et al., 2006), and pond turtles (Williamson et al., 2016), indicative of an environment much wetter than exists in the region today, with enough water to support some

aquatic ecosystems. Our $\delta^{18}O$ record indicates lower to variable wintertime precipitation in the lower Pojoaque, with increasingly winter-wet conditions occurring during the middle-upper Pojoaque where aquatic faunas are more common. $\delta^{13}C$ responds to the amount of cool-season precipitation accordingly, with soil productivity increasing steadily from 15-14 Ma. The uppermost portion of the Pojoaque records the period immediately after the MMCO, where antilocaprids and tusked deer become more common (Tedford, 1981; Williamson, 2016), reflecting a cooler, partially forested environment that agrees with the relatively high soil productivity and cooler temperatures during this time. By the last 1 myr of our isotope record, most of the fauna that existed in the Española basin during the MMCO had disappeared and the environment was mainly dominated by camels, suggesting a cooler and drier grassland environment (Tedford, 1981; Tedford and Barghoorn, 1997). The $\delta^{13}C$ record shows very low productivity during this time and the high $\delta^{18}O$ indicate a significant decrease in wintertime precipitation, with a seasonal hydroclimate balance much more similar to the modern.

Implications for Modern Climate Change

Predictions of increased aridity in the southwestern US (Overpeck and Udall 2020 (PNAS); Milly and Dunne 2020 (Science)) under warm, high pCO_2 conditions are inconsistent with our paleoclimate record. The similarity of (converted) modern $\delta^{18}O$ to mid-Miocene $\delta^{18}O$ suggests that both ENSO and NAM continue operating under these conditions and ENSO may even become stronger, as evidenced by the more winter-wet conditions of the MMCO in New Mexico. It is unclear whether this winter-wet shift is associated with a decrease in summer monsoonal precipitation, although the aridity indicated by some Española faunas may suggest that summertime precipitation did decrease. If true, the seasonal hydroclimate would have been

opposite that of the modern, with wet winters and dry summers rather than the dry winters and wet summers the region experiences today. It is also notable that the two cooler periods during the MMCO are associated with increased westerly moisture, suggesting that conditions of high pCO_2 and cooler temperatures somehow strengthen the ENSO system. Our results also point to the amount of wintertime precipitation as being a main control on ecosystem productivity and faunal makeup for the region, likely because increased recharge of groundwater during the cool season(s) makes water available year-round for plant use (Kukla et al., 2022; Knowles et al., 2018; Hu et al., 2010), supporting more biomass. Our findings for a winter-wet climate and dyamic, productive ecosystem suggest a hopeful future for the southwestern US under modern climate change, although it is unclear whether these shifts occur on time scales fast enough for human consideration.

Conclusion

We present new stable isotope records of $\delta^{18}O$ and $\delta^{13}C$ recorded in terrestrial carbonates from the Española basin in northern NM to understand the hydroclimate response to the warm, high pCO_2 conditions of the MMCO. We interpret $\delta^{18}O$ as reflecting the balance between wintertime and summertime precipitation (or westerly/ENSO-derived precipitation and monsoonal precipitation, respectively), and $\delta^{13}C$ as a measure of soil productivity. The age model applied to the records is calculated from new and updated $^{40}Ar/^{39}Ar$ ages of nine ash units in the basin, developing a high-resolution record of environmental change in the Española basin across the MMCO. From 17-13.9 Ma, carbonate $\delta^{18}O$ decreases by ~2‰, indicating a shift towards a more winter-wet climate in the region; this decrease over time is comprised of individual $\delta^{18}O$ minima and maxima that likely represent interannual variability of the seasonal precipitation balance, likely influenced at least in part by changing amounts in precipitation delivered to the region by ENSO. In comparison to modern precipitation $\delta^{18}O$, Española $\delta^{18}O$ during the MMCO is similar but more negative, indicating that the seasonal hydroclimate was not very different from today, but received more ENSO-derived, cool-season precipitation. The $\delta^{18}O$ and $\delta^{13}C$ records are highly correlated, indicating a common driver between the two signals; we find that soil productivity increased when the hydroclimate was more winter-wet, indicating that wintertime precipitation is a strong control on soil productivity in the region. We also find that soil productivity did not have one linear response to MMCO conditions, but rather shorter-term, dynamic responses to the seasonal precipitation balance that likely led to a variety of vegetation in the basin throughout the MMCO. This is in good agreement with the Española fossil record, which indicates a wide variety of herbivores that would have fed on a range of vegetation types. The faunal fossil record also indicates that periods of increased cool-season precipitation and

higher soil productivity are associated with higher faunal diversity, showing a larger ecosystem response to hydroclimate change. Overall, we find evidence for a productive ecosystem with an increasingly winter-wet hydroclimate rather than evidence for increased aridity in the southwest US during the warm, high pCO_2 (~400-600 ppm) mid-Miocene.

Table 1
New 40Ar/39Ar Ages
*Age obtained using a sample from outside the study area that was correlated to the ash in our study site through tephrachronological analysis.
WASH: West Arroyo Seco Hanging Wall Section

Ash Unit	Original description	Location (UTM, NAD83, 13N)	Stratigraphic position	Section	Previous age (Ma)	Previous age source	New age (Ma; $^{40}Ar/^{39}Ar$)
Lower Nambé white ash	Koning et al., 2005	414183 m E, 3982083 m N	33 m below 0 m on our section	Nambé	---	---	17.416 ± 0.013
Nambé white ash*	Galusha and Blick, 1971	Dan's or my coordinates?	65 m	Nambé	16.4 ± 0.13	Izett & Obradovich, 2000	16.523 ± 0.022
White Ash No. 2	Galusha and Blick, 1971	411081 m E, 3978427 m N	48 m	WASH	---	---	16.02 ± 0.12
White Ash No. 3	Galusha and Blick, 1971	411064 m E, 3978417 m N	68.5	WASH	15.5 ± 0.07 14.6 ± 1.2	Izett & Obradovich, 2000 Izett & Naeser, 1981	15.857 ± 0.041
White Ash E	Koning et al., 2005	410902 m E, 3978426 m N	83.9	WASH	---	---	15.783 ± 0.022
White Ash No. 4	Galusha and Blick, 1971	410344 m E, 3979148 m N	175	WASH	15.3 ± 0.05, 14.2 ± 0.03; 14.1 ± 1.1, 12.7 ± 1.4; 15.42 ± 0.06	Izett & Obradovich, 2000; Izett & Naeser, 1981; McIntosh & Quade, 1995	15.463 ± 0.026
Road Ash*	Izett & Obradovich, 2000	Dan's or mine?	26	La Puebla	15.1 ± 0.06	Izett & Obradovich, 2000	15.343 ± 0.031
Pojoaque White Ash	Galusha and Blick, 1971	411699 m E, 3988121 m N	152	Pojoaque	13.7 ± 0.18	Izett & Obradovich, 2000	13.602 ± 0.028
Pojoaque Blue Gray Ash	Galusha and Blick, 1971	405980 m E, 3975144 m N	153	Pojoaque	---	---	13.77 ± 0.21

Table 2: $\delta^{18}O$ Analysis of Variance Table

	df	Sum of Squares	Mean Square	F	Sig.
Sample type	3	51.05	17.0169	8.1016	3.212e-5
Residuals	325	681.45	2.0968		

Table 3: $\delta^{18}O$ Pairwise comparison using estimated marginal means

Sample type	Estimated Marginal Means	Standard Error	df	Lower Bound (95% CI)	Upper Bound (95% CI)	Group
Rhizolith	-11.4	0.192	326	-11.7	-11.0	1
Cement	-11.2	0.146	326	-11.5	-11.0	1
Matrix	-10.9	0.211	326	-11.3	-10.5	1 2
Nodule	-10.4	0.129	326	-10.7	-10.2	2

Table 4: $\delta^{13}C$ Analysis of Variance Table

	df	Sum of Squares	Mean Square	F	Sig.
Sample type	3	6.969	2.32304	4.8964	0.002421
Residuals	325	154.194	0.47444		

Table 5: $\delta^{13}C$ Pairwise comparison using estimated marginal means

Sample type	Estimated Marginal Means	Standard Error	df	Lower Bound (95% CI)	Upper Bound (95% CI)	Group
Rhizolith	-6.10	0.0908	325	-6.27	-5.92	1
Cement	-5.88	0.0689	325	-6.02	-5.75	1 2
Nodule	-5.72	0.0611	325	-5.84	-5.60	2
Matrix	-5.66	0.1011	325	-5.86	-5.47	2

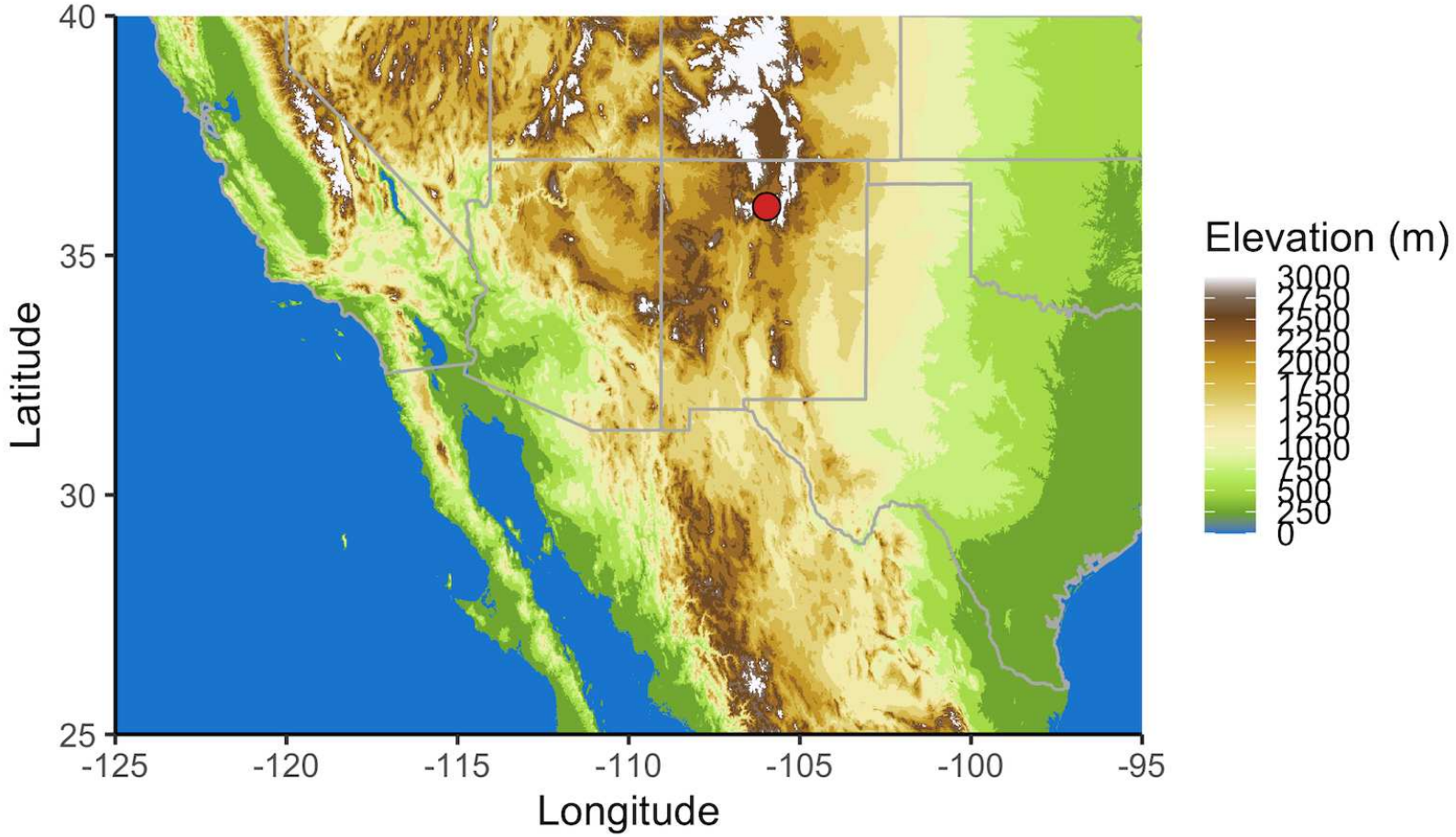

Figure 1: The Española basin is a relatively low elevation area with high topography on both sides: the Sangre de Cristo range to the east and the Jemez range to the west.

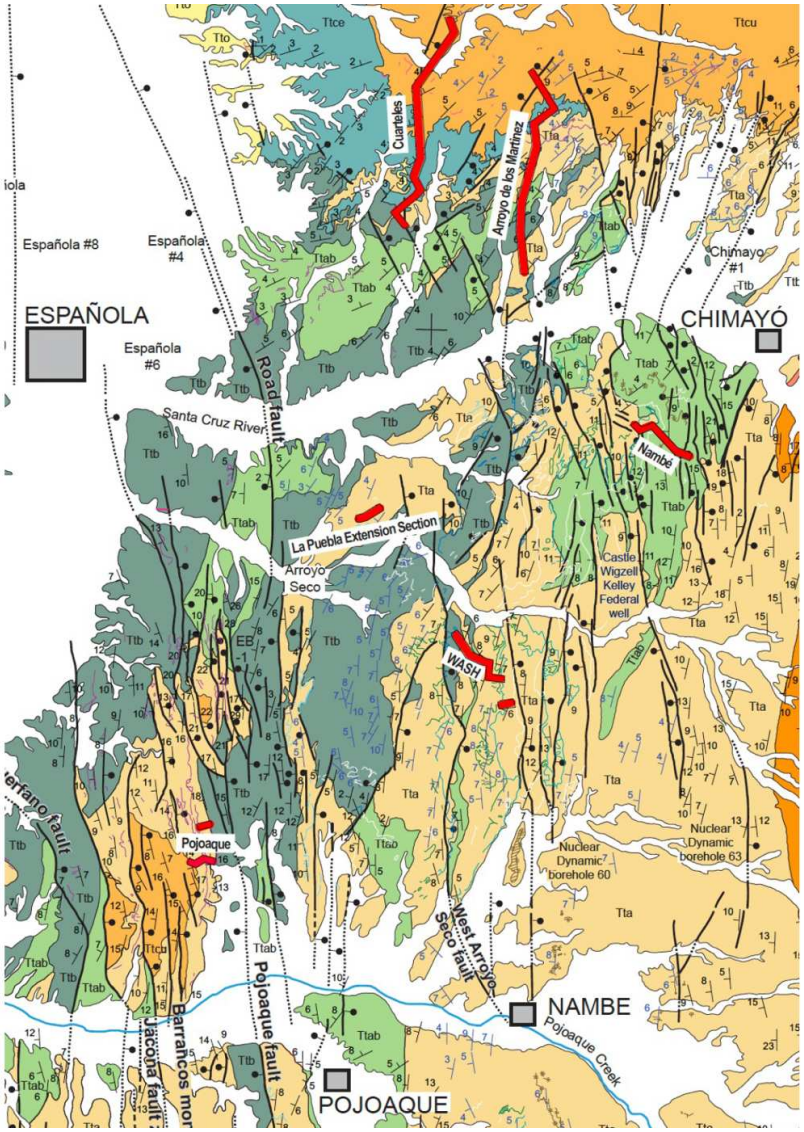

Figure 2: The locations of the stratigraphic sections sampled for this study, located between Española, Chimayó, and the Nambé and Pojoaque Pueblos. This figure is a geologic map taken from Koning et al., 2013.

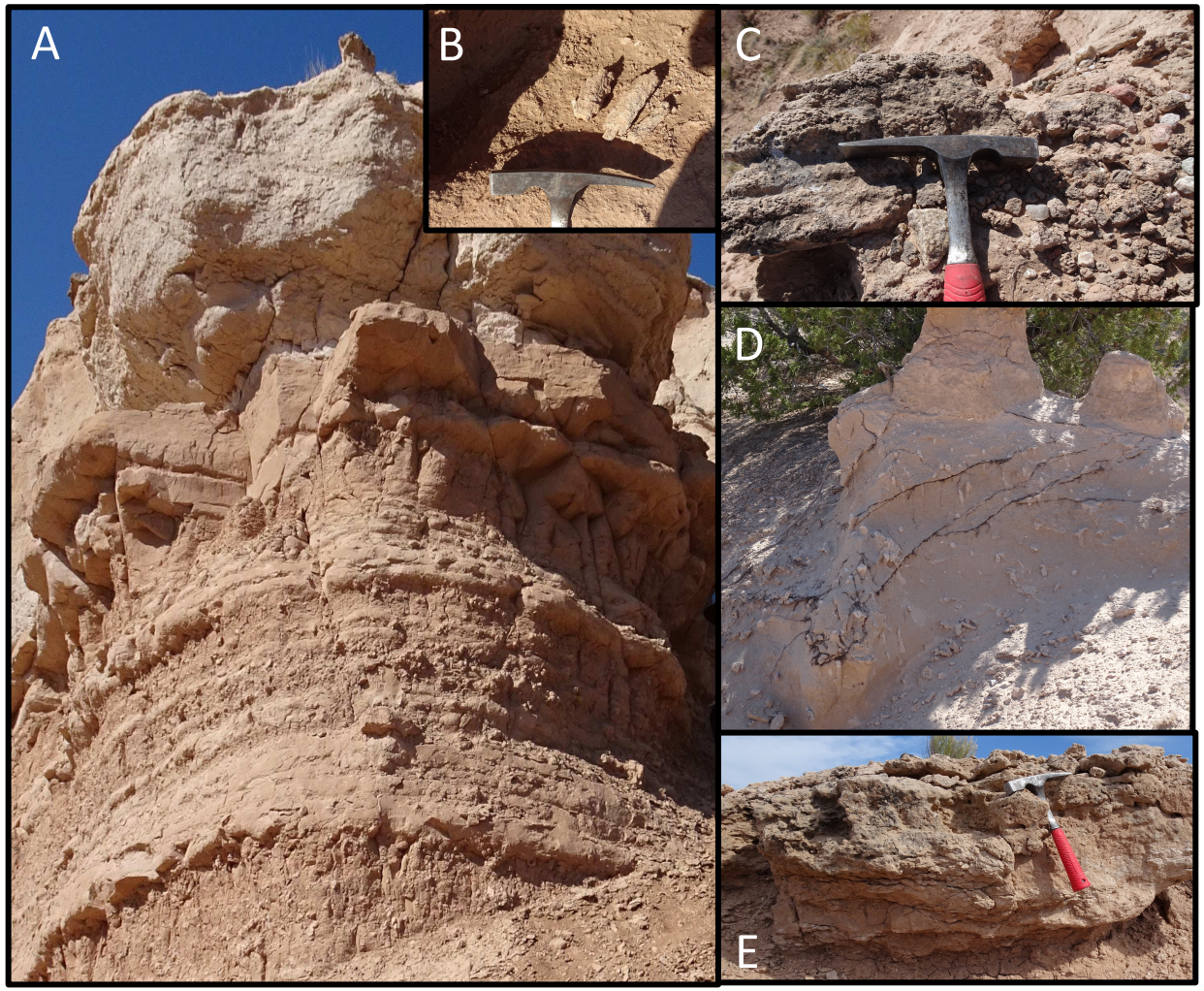

Figure 3: (A) Carbonate nodules can be seen weathering out of the lower siltstone units with a carbonate cemented layer (sampled as cement) forming the resistant cap at the top of the photo. (B) Example of rhizolith samples. (C) Example of highly carbonate cemented sediment with directional features thought to indicate cementation by groundwater flow, sampled as cement. (D) Rhizoliths seen weathering out of a siltstone. (E) Example of ledge-forming cement.

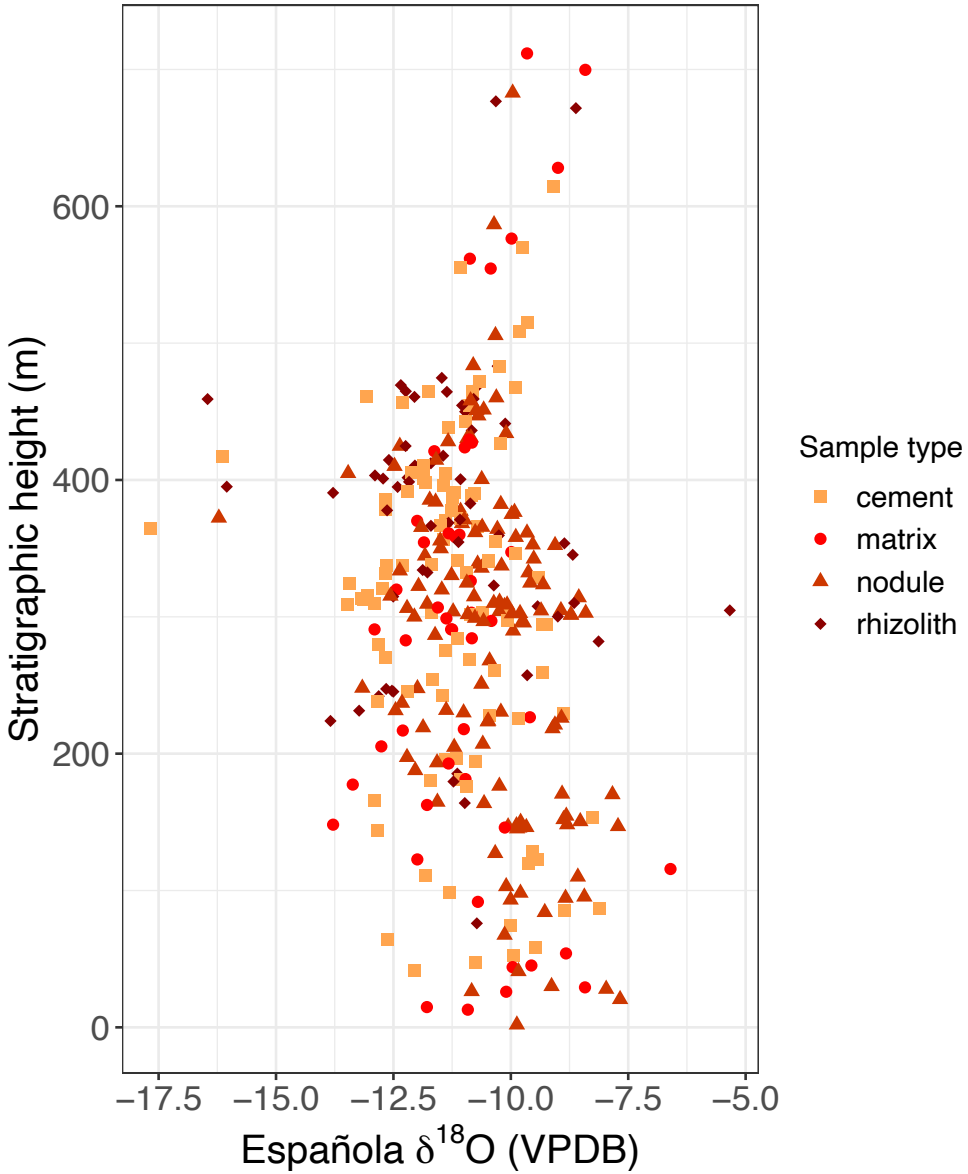

Figure 4: $\delta^{18}O$ by stratigraphic height colored by sample type.

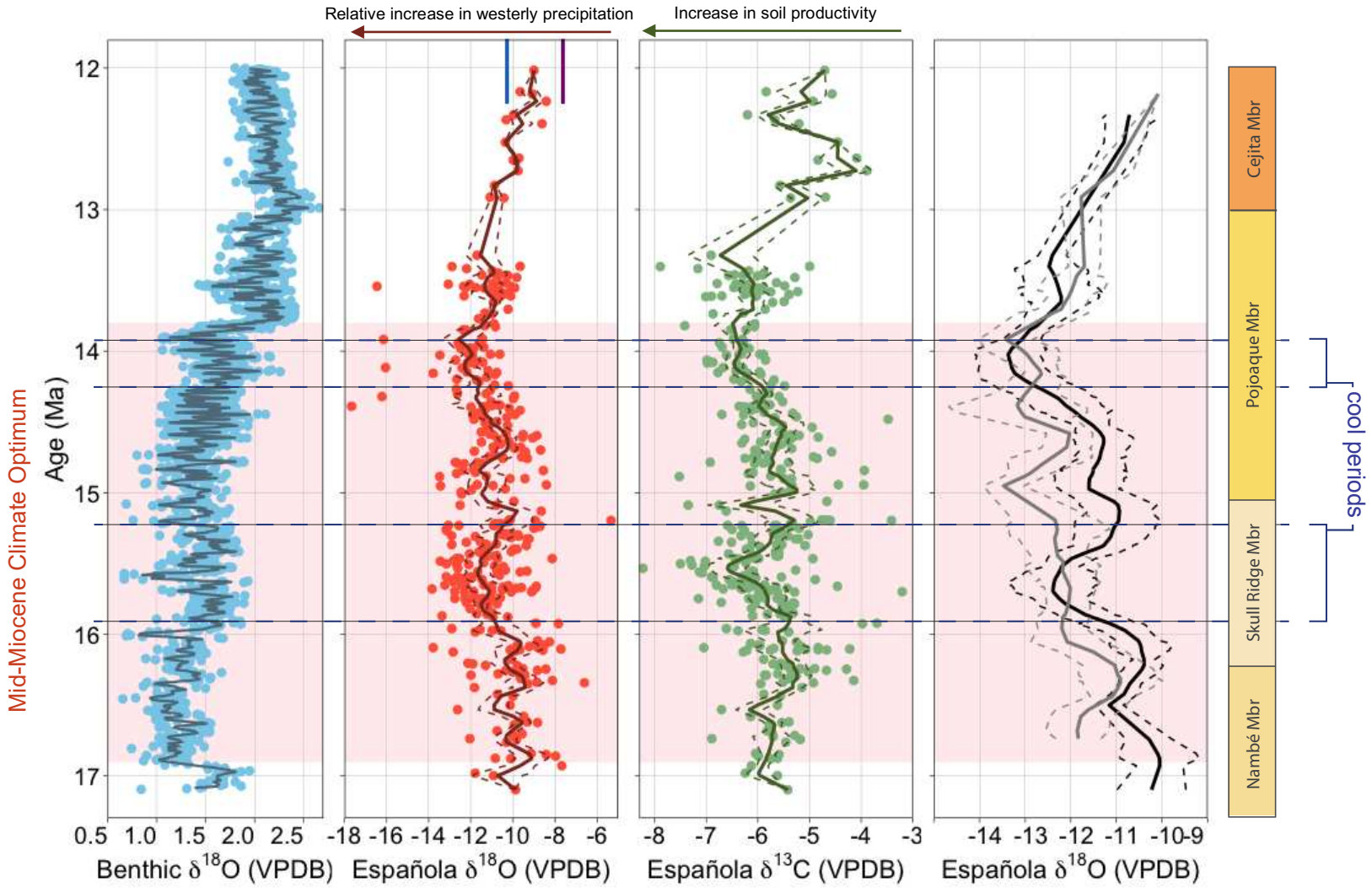

Figure 5: Benthic $\delta^{18}O$ record from DeVleeschouwer et al. (2017) compared to measured $\delta^{18}O$ and $\delta^{13}C$ of Española carbonates. The blue and purple lines at the top of the $\delta^{18}O$ plot represent the average modern precipitation $\delta^{18}O$ converted into its equivalent carbonate value at T=19°C (assuming no seasonal carbonate formation bias) and T=28°C (assuming a summer formation bias).

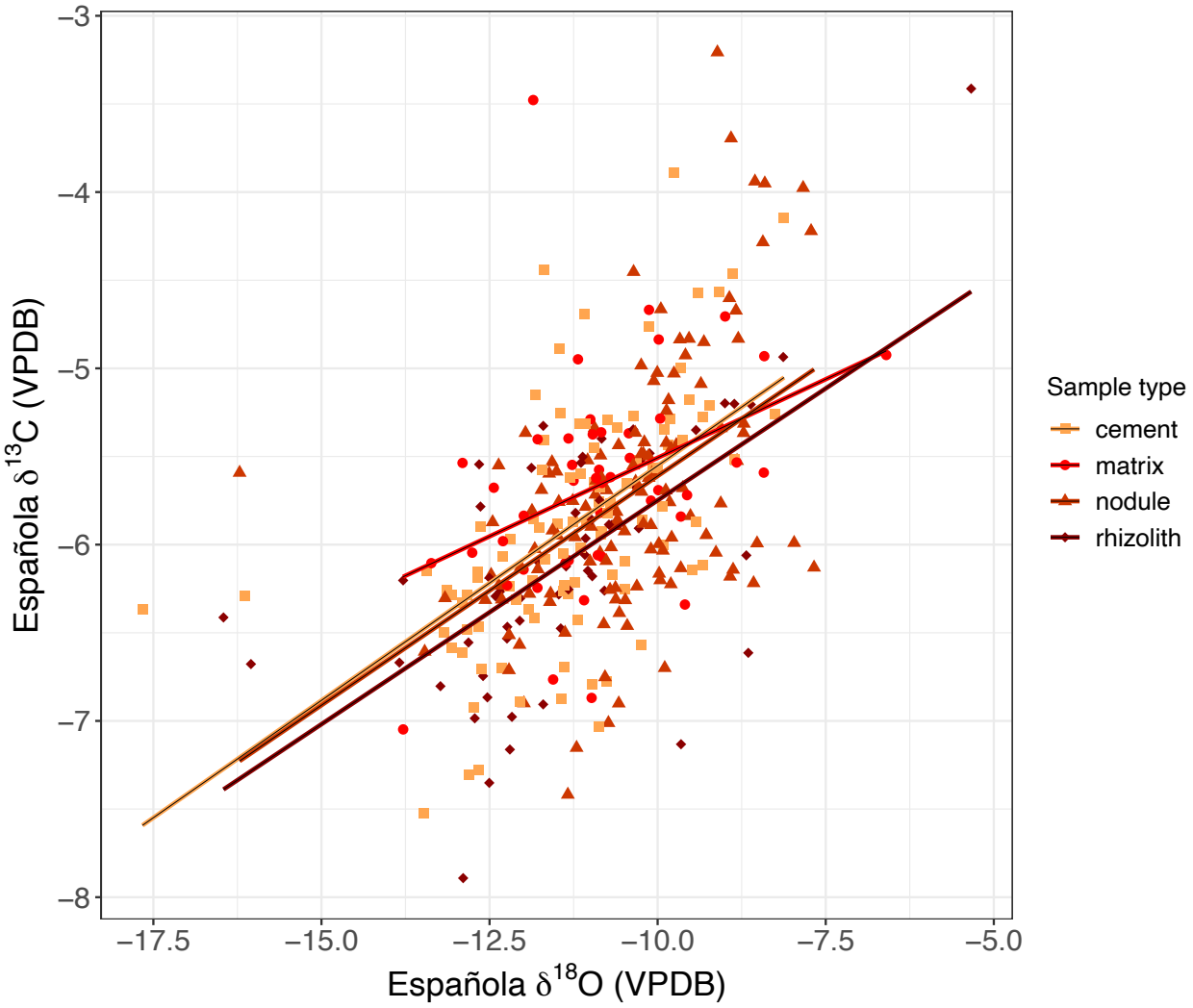

Figure 6: Comparison of $\delta^{18}O$ and $\delta^{13}C$ by carbonate sample type; indicates no apparent bias.

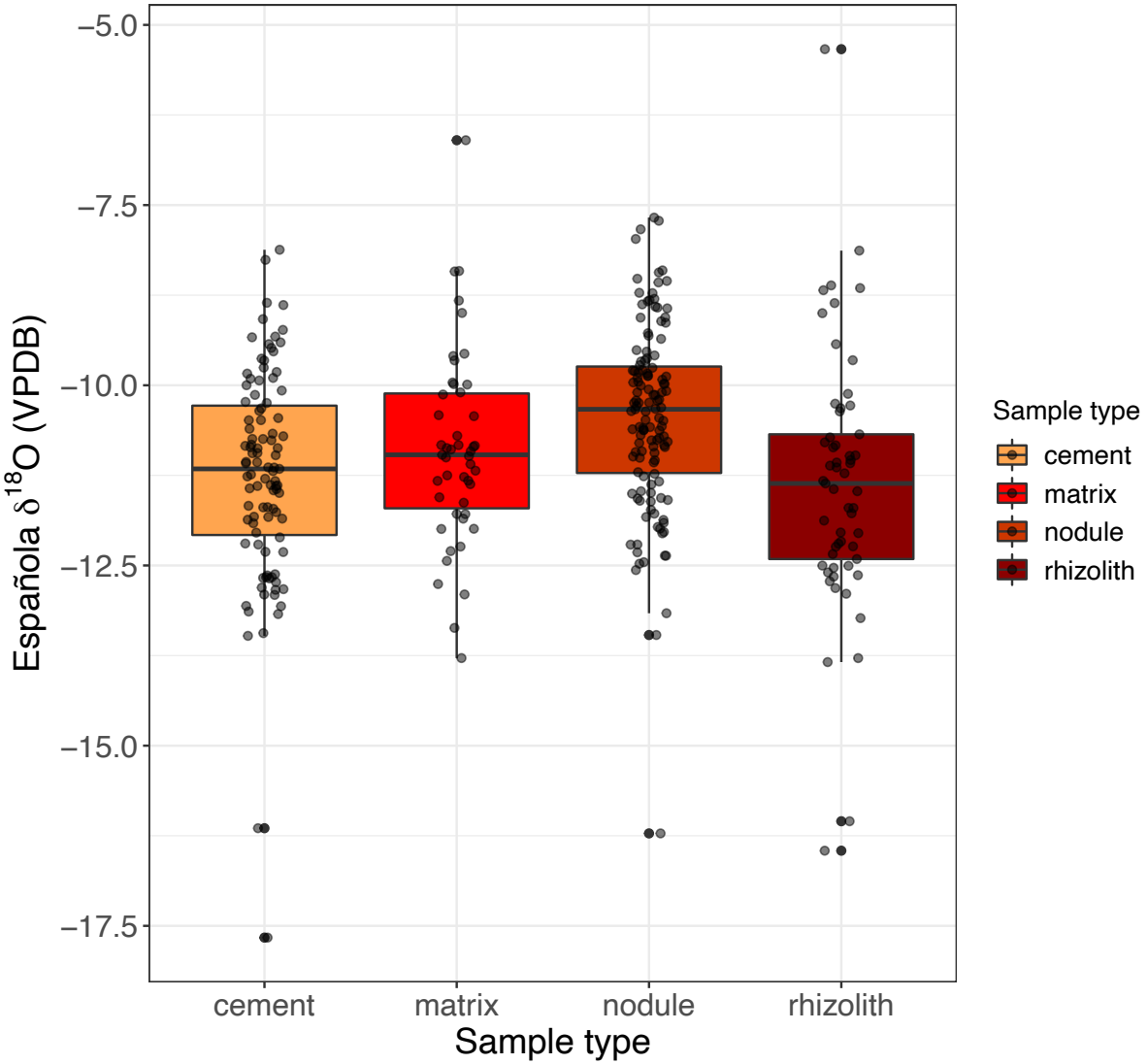

Figure 7: Comparison of $\delta^{18}O$ by carbonate sample type. Statistical analysis reveals two groups of statistically similar means: *(1)* rhizoliths, cements, and matrix samples, and *(2)* matrix and nodules.

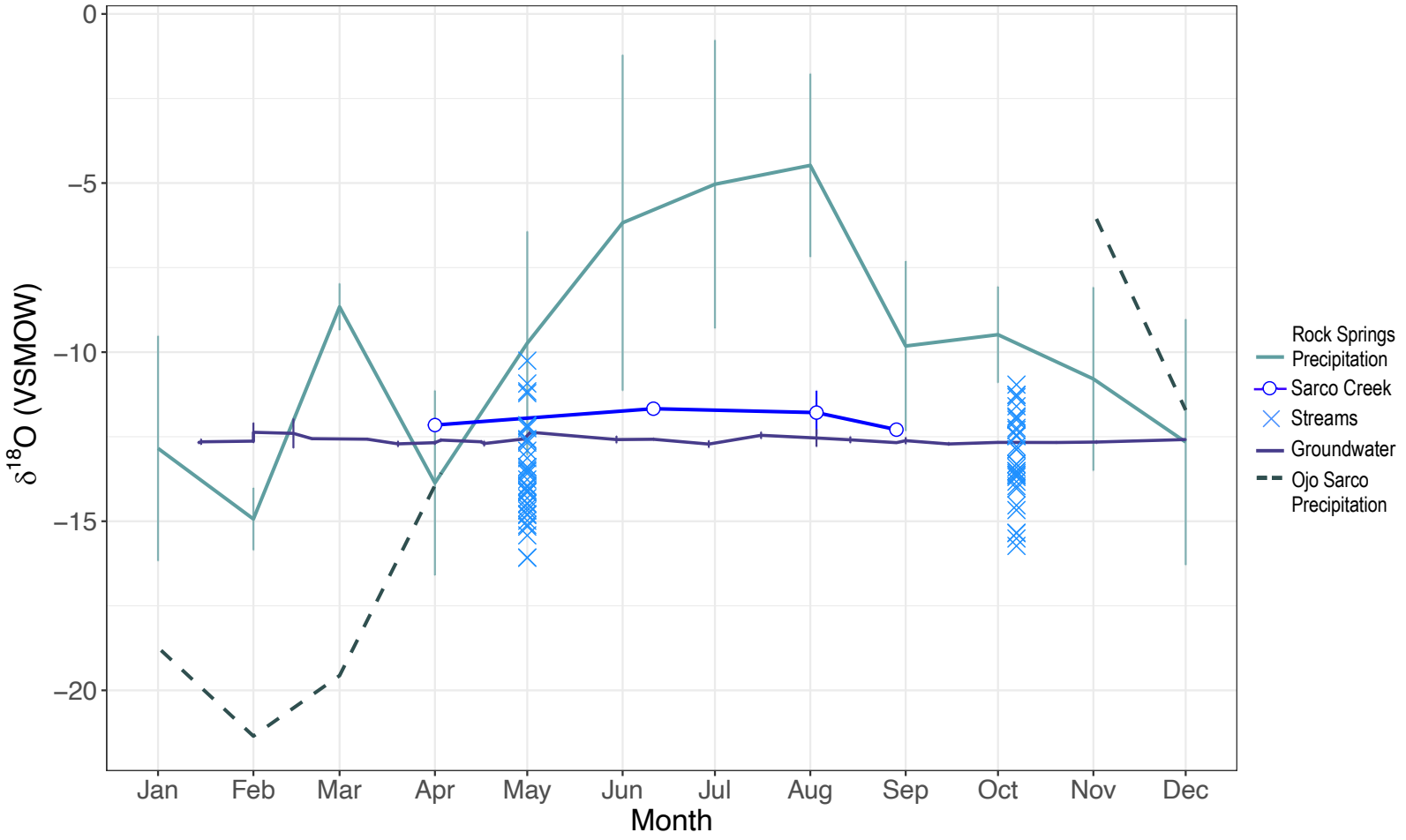

Figure 8: Annual $\delta^{18}O$ record of Rock Springs, NM, precipitation (Tulley-Cordova et al., 2021) and Ojo Sarco, NM, groundwater; partial records of Sarco Creek (Ojo Sarco) and Ojo Sarco precipitation; and $\delta^{18}O$ values of individual streams in northern NM and southern CO sampled during different times of year.

References

Aby, S. B., Morgan, G. S., Koning, D. J., 2011, A paleontological survey of a part of the Tesuque Formation near Chimaya, New Mexico, and a summary of the biostratigraphy of the Pojoaque Member (Middle Miocene, Late Barstovian), in Koning, D. J., Karlstrom, K. E., Kelley, S. A., Lueth, V. W., Aby, S. B., New Mexico Geological Society 62nd Annual Fall Field Conference Guidebook, p. 418.

Axelrod, D. I, Bailey, H. P., 1976, Tertiary Vegetation, Climate, and Altitude of the Rio Grande Depression, New Mexico-Colorado: Paleobiology, v. 2, p. 235-254, doi:10.1017/S0094837300004814.

Barghoorn, S., 1981, Magnetic-polarity stratigraphy of the Miocene type Tesuque Formation, Santa Fe Group, in the Española Valley, New Mexico: Geological Society of America Bulletin, v. 92, p. 1027–1041, doi:10.1130/0016-7606(1981)92<1027:MSOTMT>2.0.CO;2.

Barghoorn, S., 1985, Magnetic polarity stratigraphy of the Tesuque Formation, Santa Fe Group in the Española Valley, New Mexico, with a taxonomic review of fossil camels [PhD dissertation]: Columbia University, New York, 430 p.

Breecker, D.O., Sharp, Z.D. and McFadden, L.D., 2009, Seasonal bias in the formation and stable isotopic composition of pedogenic carbonate in modern soils from central New Mexico, USA: Geological Society of America Bulletin, v. 121, pp.630-640, doi: 10.1130/B26413.1.

Burls, N. J., Fedorov, A. V., 2017, Wetter subtropics in a warmer world: Contrasting past and future hydrological cycles: Proceedings of the National Academy of Sciences, v. 28, p. 12,888-12,893, doi:10.173/pnas.1703421114.

Cavazza, W., 1986, Miocene sediment dispersal in the central Española Basin, Rio Grande rift, New Mexico, USA: Sedimentary Geology, v. 51, p. 119-135.

Caves, J. K., Winnick, M. J., Graham, S. A., Sjostrom, D. J., Mulch, A., Chamberlain, C. P., 2015, Role of the westerlies in Central Asia climate over the Cenozoic: Earth Planetary Science Letters, v. 428, p. 33-43, doi:10.1016/j.epsl.2015.07.023.

Cerling, T.E., 1984, The stable isotopic composition of modern soil carbonate and its relationship to climate: Earth and Planetary science letters, v. 71, pp.229-240, doi: 10.1016/0012-821X(84)90089-X.

Coats, S., Karnauaskas, K. B., 2017, Are Simulated and Observed Twentieth Century Tropical Pacific Sea Surface Temperature Trends Significant Relative to Internal Variability?: Geophysical Research Letters, v. 44, p. 9928-9937, doi:10.1002/2017GL074622.

Cope, E. D., 1877, Report upon the extinct Vertebrata obtained in New Mexico by parties of the expedition of 1874, in Wheeler, G. M., Report upon United States Geological Surveys West of the One Hundredth Meridian: Washington, v. 4, pt. 2, p. 1-370.

De Vleeschouwer, D., Vahlenkamp, M., Crucifix, M., Pälike, H., 2017, Alternating Southern and Northern Hemisphere climate response to astronomical forcing during the past 35 m.y.: Geology, v. 45, p. 375-378, doi: 10.1130/G38663.1.

Douville, H., Raghavan, K., Renwick, J., Allan, R.P., Arias, P. A., Barlow, M., Cerezo-Mota, R., Cherchi, A., Gan, T. Y., Gergis, J., Jiang, D., Khan, A., Pokam Mba, W., Rosenfeld, D., Tierney, J., Zolina, O., 2021, Water Cycle Changes, in: Masson-Delmotte, V., Zhai, P., Pirani, A., Connors, S. L., Péan, C., Berger, S., Caud, N., Chen, Y., Goldfarb, L., Gomis, M. I., Huang, M., Leitzell, K., Lonnoy, E., Matthews, J. B. R., Maycock, T. K., Waterfield, T., Yelekçi, O., Yu, R., Zhou, B., (Eds.), Climate Change 2021: The Physical Science Basis. Contribution of Working Group I to the Sixth Assesment Report of the Intergovernmental Panel on Climate Change: Cambridge University Press, p. 239.

Farquhar, G. D., Ehleringer, J. R., Hubick, K. T., 1989, Carbon isotope discrimination and photosynthesis: Annual review of plant physiology and plant molecular biology, v. 40, p. 503-537.

Fedorov, A. V., Brierley, C. M., Lawrence, K. T., Liu, Z., Dekens, P. S., Ravelo, A. C., 2013, Patterns and mechanisms of early Pliocene warmth: Nature, v. 496, p. 43-49, doi:10.1038/nature12003.

Frick, C., 1926a, Prehistoric evidence: Natural History, v. 26, p. 440-448.

Galusha, T., and Blick, J.C., 1971, Stratigraphy of the Santa Fe Group, New Mexico: Bulletin of the American Museum of Natural History, v. 144, 127 p.

Galeotti, S., Von der Heydt, A., Huber, M., Bice, D., Dijkstra, H., Jilbert, T., Lanci, L. and Reichart, G.J., 2010, Evidence for active El Niño Southern Oscillation variability in the Late Miocene greenhouse climate: Geology, v. 38, p. 419-422.

Goldner, A., Herold, N. and Huber, M., 2014, The challenge of simulating the warmth of the mid-Miocene climatic optimum in CESM1: Climate of the Past, v. 10, pp.523-536, doi: 10.5194/cp-10-523-2014.

Guillermic, M., Misra, S., Eagle, R., Tripati, A., 2022, Atmospheric CO2 estimates for the Miocene to Pleistocene based on foraminiferal $\delta^{11}B$ at Ocean Drilling Program Sites 806 and 807 in the Western Equatorial Pacific: Climate of the Past, v. 18, p. 183-207, doi:10.5194/cp-18-183-2022.

Harris, E. B., 2016, Effects of the mid-Miocene climatic optimum on ecosystem structure and plant-animal interactions: A phytolith and stable isotope perspective, Ph.D. Dissertation: Department of Biology, University of Washington.

Haug, G. H., Tiedemann, R., Zahn, R., Ravelo, A. C., 2001, Role of Panama uplift on oceanic freshwater balance: Geology, v. 29, p. 207-210, doi:10.1130/0091-7613(2001)029<0207:ROPUOO>2.0CO;2

Haywood, A. M., Dowsett, H. J., Dolan, A. M., 2016, Integrating geological archives and climate models for the mid-Pliocene warm period: Nature Communications, doi: 10.1038/ncomms10646.

Hu, H., Dominguez, F., 2015, Evaluation of Oceanic and Terrestrial Sources of Moisture for the North American Monsoon Using Numerical Models and Precipitation Stable Isotopes: Journal of Hydrometeorology, v. 16, p.19-35, doi: 10.1175/JHM-D-14-0073.1.

Ibarra, D. E., Oster, J. L., Winnick, M. J., Caves Rugenstein, J. K., Byrne, M. P., Chamberlain, C. P., 2018, Warm and cold wet states in the western United States during the Pliocene – Pleistocene: Geology, v. 48, p. 355-358, doi:10.1130/G39962.1.

Izett, G. A., and Naeser, C. W., 1981, Fission-track ages of air-fall tuffs in Miocene sedimentary rocks of the Espanola Basin, Santa Fe County, New Mexico: US Geological Survey Open File Report 81-161.

Izett, G.A., and Obradovich, J.D., 2001, 40Ar/39Ar ages of Miocene tuffs in basinfill deposits (Santa Fe Group, New Mexico, and Troublesome Formation, Colorado) of the Rio Grande rift system: The Mountain Geologist, v. 38, no. 2, p. 77-86.

Kim, S., O'Neill, J. R., 1997, Equilibrium and nonequilibrium oxygen isotope effects in synthetic carbonates: Geochimica et Cosmochimica Acta, v. 61, p. 3461-3475, doi: 10.1016/S0016-7037(97)00169-5.

Knowles, J.F., Molotch, N.P., Trujillo, E. and Litvak, M.E., 2018, Snowmelt-driven trade-offs between early and late season productivity negatively impact forest carbon uptake during drought: Geophysical Research Letters, v. 45, p.3087-3096.

Koning, D.J., Connell, S.D., Morgan, G.S., Peters, L., and McIntosh, W.C., 2005, Stratigraphy and depositional trends in the Santa Fe Group near Española, north-central New Mexico: tectonic and climatic implications: New Mexico Geological Society, 56th Field Conference Guidebook, Geology of the Chama Basin, p. 237-257.

Koning, D.J., Grauch, V.J.S., Connell, S.D., Ferguson, J., McIntosh, W., Slate, J.L., Wan., E., and Baldridge, W.S., 2013, Structure and tectonic evolution of the eastern Española Basin, Rio Grande rift, north-central New Mexico, in Hudson, M., and Grauch, V.J.S., eds., New Perspectives on the Rio Grande rift: From Tectonics to Groundwater: Geological Society of America, Special Paper 494, p. 185-219, doi:10.1130/2013.2494(08).

Krapp, M., and Jungclaus, J. H., 2011, The Middle Miocene climate as modelled in an atmosphere-ocean-biosphere model: Clim. Past, v. 7, p. 1169-1188., doi: 10.5194/cp-7-1169-2011.

Krapp, M., and Jungclaus, J. H., 2015, Pacific variability under present-day and Middle Miocene boundary conditions: Clim Dyn, v. 44, p. 2609-2621, doi: 10.1007/s00382-014-2456-2.

Kues, B. S., and Lucas, S. G., 1979, Summary of the paleontology of the Santa Fe Group (Mio-Pliocene), north-central New Mexico: New Mexico Geological Society, 30th Field Conference Guidebook, p. 237-241.

Kukla, T., Rugenstein, J.K.C., Ibarra, D.E., Winnick, M.J., Strömberg, C.A. and Chamberlain, C.P., 2022, Drier winters drove Cenozoic open habitat expansion in North America: AGU Advances, v. 3, doi:10.1029/2021AV000566.

Lunt, D. J., Valdes, P. J., Haywood, A., Rutt, I. C., 2008, Closure of the Panama Seaway during the Pliocene: Implications for climate and Northern Hemisphere glaciation: Climate Dynamics, v. 30, p. 1-18, doi:10.1007/s00382-007-0265-6.

Mankin, J. S., Smerdon, J. E., Cook, B. I., Williams, A. P., Seager, R., 2017, The curious case of projected 21st-century drying but greening in the American West: Journal of Climate, doi:10.1175/JCLI-D-17-0213.1.

McIntosh, W. C., and Quade, J., 1995, 40Ar/39Ar geochronology of tephra layers in the Santa Fe group, Española Basin, New Mexico: New Mexico Geological Society, 46th Field Conference Guidebook, Geology of the Santa Fe Region, p. 279-287.

McKinney, K. C., Chaney, D. S., Maldonado, F., 2006, Preliminary report on the newly discovered Miocene flora of Pojoaque bluffs, Española Basin, north-central New Mexico, in McKinney, K. C., Geologic and Hydrogeologic Framework of the Española Basin -- Proceedings of the 5th Annual Española Basin Workshop, Santa Fe, New Mexico, March 7-8, 2006, p. 32.

McPhaden, M. J., Zebiak, S. E., Glantz, M. H., 2006, ENSO as an Integrating Concept in Earth Science: Science, v. 314, p. 1740-1745, doi:10.1126/science.1132588.

Methner, K., Mulch, A., Fiebig, J., Krsnik, E., Löffler, N., Bajnai, D., Chamberlain, C. P., 2021, Warm High-Elevation Mid-Latitudes During the Miocene Climate Optimum: Paleosol Clumped Isotope Temperatures From the Northern Rocky Mountains, USA: Paleoceanography and Paleoclimatology, v. 36, doi:10.1029/2020PA003991.

Mix, H. T., Chamberlain, C. P., 2014, Stable isotope records of hydrologic change and paleotemperature from smectite in Cenozoic western North America: Geochimica et Cosmochimica Acta, v. 141, p. 532-546, doi:10.1016/j.gca.2014.07.008.

Morgan, G. S., 2015, Oligocene and Miocene Vertebrates of New Mexico: New Mexico Museum of Natural History and Science Bulletin 68, p. 159-232.

Ogg, J. G., 2020, Geomagnetic polarity time scale, in Geologic time scale 2020, Elsevier, p. 159-192, doi: 10.1016/B978-0-12-824360-2.00005-X.

O'Leary, M. H., 1988, Carbon Isotopes in Photosynthesis: BioScience, v. 38, p. 328-336, doi:10.2307/1310735.

Olonscheck, D., Rugenstein, M., Marotzke, J., 2020, Broad Consistency Between Observed and Simulated Trends in Sea Surface Temperature Patterns: Geophysical Research Letters, v. 47, doi:10.1029/2019GL086773.

Pound, M. J., Haywood, A. M., Salzmann, U., Riding, J. B., 2012, Global vegetation dynamics and latitudinal temperature gradients during the Mid to Late Miocene (15.97-5.33 Ma): Earth Science Reviews, v. 112, p. 1-22, doi:10.1016/j.earscirev.2012.02.005.

Quade, T.C.J., 1993, Stable carbon and oxygen isotopes in soil carbonates: Climate change in continental isotopic records: Geophysical Monograph, v. 78, pp.217-231.

Rugenstein, J. K. C., Chamberlain, C. P., 2018, The evolution of hydroclimate in Asia over the Cenozoic: A stable-isotope perspective: Earth-Science Reviews, v. 185, p. 1129-1156, doi:10.1016/j.earscirev.2018.09.003.

Scheff, J., Seager, R., Liu, H., Coats, S., 2017, Are glacials dry? Consequences for paleoclimatology and for greenhouse warming: Journal of Climate, v. 30, p.6593-6609, doi:10.1175/JCLI-D-16-0854.1.

Schmidt, D. F., Grise, K. M., 2021, Drivers of Twenty-First Century U.S. Winter Precipitation Trends in CMIP6 Models: A Storyline-Based Approach, Journal of Climate, v. 34, p. 6875-6889, doi:10.1175/jcli-d-21-0080.1.

Scott, R.L., Shuttleworth, W.J., Keefer, T.O. and Warrick, A.W., 2000, Modeling multiyear observations of soil moisture recharge in the semiarid American Southwest: Water Resources Research, v. 36, p.2233-2247, doi:10.1029/2000WR900116.

Seager, R., Cane, M., Henderson, N., Lee, D. E., Abernathey, R., Zhang, H., 2019, Strengthening tropical Pacific zonal sea surface temperature gradient consistent with rising greenhouse gases: Nature Climate Change, v. 9, p. 517-522, doi:10.1038/s41558-019-0505-x.

Seager, R., Vecchi, G. A., 2010, Greenhouse warming and the 21st century hydroclimate of southwestern North America: Proceedings of the National Academy of Sciences, v. 107, p. 21277-21282, doi:10.1073/pnas.0910856107.

Simpson, I. R., McKinnon, K., Davenport, F., Tingley, M., Lehner, F., Fahad, S., Chen, D., 2021, Emergent Constraints on the Large-Scale Atmospheric Ciruclation and Regional Hydroclimate: Do They Still Work in CMIP6 and How Much Can They Actually Constrain the Future?: Journal of Climate, v. 34, p. 6355-6377, doi:10.1175/JCLI-D-21-0055.1.

Sheppard, P., Comrie, A. C., Packin, G., Angersbach, K., Hughes, M., 2002, The Climate of the U.S. Southwest: Climate Research, v. 21, p. 219-318, doi:10.3354/cr021219.

Slate, J.L., Sarna-Wojcicki, A.M., Koning, D.J., Wan, E., Wahl., D., Connell, S.D., and Perkins, M.E., 2013, Upper Neogene tephrochronologic correlations of the Española Basin and Jemez Mountains volcanic field, northern Rio Grande rift, north-central New Mexico, in Hudson, M.,

and Grauch, V.J.S., eds., New Perspectives on the Rio Grande rift: From Tectonics to Groundwater: Geological Society of America, Special Paper 494, p. 303-322, doi:10.1130/2013.2494(12).

Steinthorsdottir, M., Coxall, H.K., De Boer, A.M., Huber, M., Barbolini, N., Bradshaw, C.D., Burls, N.J., Feakins, S.J., Gasson, E., Henderiks, J. and Holbourn, A.E., 2021, The Miocene: The future of the past: Paleoceanography and Paleoclimatology, v. 36, doi: 10.1029/2020PA004037.

Steinthorsdottir, M., Jardine, P. E., Rember, W. C., 2021, Near-Future pCO2 During the Hot Miocene climate Optimum: Paleoceanography and Paleoclimatology, v. 36, doi:10.1029/2020PA003900.

Spötl, C., Wright, V. P., 1992, Groundwater dolocretes from the Upper Triassic of the Paris Basin, France: a case study of an arid, continental diagenetic facies: Sedimentology, v. 39, p. 1119-1136, doi:10.1111/j.1365-3091.1992.tb02000.x.

Swann, A. L. S., Hoffman, F. M., Koven, C. D., Randerson, J. T., 2016, Plant responses to increasing CO2 reduce estimates of climate impacts on drought severity: Proceedings of the National Academy of Sciences, v. 113, p. 10019-10024, doi:10.1073/pnas.1604581113.

Tang, G., Arnone III, J. A., Verburg, P. S. J., Jasoni, R. L., and Sun, L., 2015, Trends and climatic sensitivities of vegetation phenology in semiarid and arid ecosystems in the US Great Basin during 1982–2011: Biogeosciences, v. 12, p. 6985–6997, doi:10.5194/bg-12-6985-2015.

Tedford, R.H., 1981, Mammalian biochronology of the late Cenozoic basins of New Mexico: Geological Society of America Bulletin, v. 92, p.1008-1022, doi: 10.1130/0016-7606(1981)92<1008:MBOTLC>2.0.CO;2.

Tedford, R.H., and Barghoorn, S., 1997, Miocene mammals of the Espanola and Albuquerque basins, North-central New Mexico in, Lucas, SG, Estep, JW, Williamson, TE, and Morgan, GS, eds., New Mexico's Fossil Record, 1, pp.77-96.

Tulley-Cordova, C. L., Putman, A. L., Bowen, G. J., 2021, Stable Isotopes in Precipitation and Meteoric Water: Sourcing and Tracing the North American Monsoon in Arizona, New Mexico, and Utah: Water Resources Research, v. 57, doi:10.1029/2021WR030039.

Winnick, M. J., Welker, J. M., Chamberlain, C. P., 2013, Stable isotopic evidence of El Niño-like atmospheric circulation in the Pliocene western United States: Climate of the Past, v. 9, p. 903-912, doi:10.5194/cp-9-903-2013.

Williamson, G., 2016, The stratigraphic position of fossil vertebrates from the Pojoaque Member of the Tesuque Formation (Middle Miocene, Late Barstovian) near Española, New Mexico [Master's dissertation]: Stephen F. Austin State University, Texas.

Zhang, X., Prange, M., Steph, S., Butzin, M., Krebs, U., Lunt, D. J., Nisancioglu, K. H., Park, W., Schmittner, A., Schneider, B., Schulz, M., 2012, Changes in equatorial Pacific thermocline

depth in response to Panamanian seaway closure: Insights from a multi-model study: Earth Planetary Science Letters, v. 317-318, p. 76-84, doi:10.1016/j.epsl.2011.11.028.

Zhang, X., Prange, M., Steph, S., Butzin, M., Krebs, U., Lunt, D.J., Nisancioglu, K.H., Park, W., Schmittner, A., Schneider, B. and Schulz, M., 2012, Changes in equatorial Pacific thermocline depth in response to Panamanian seaway closure: Insights from a multi-model study: Earth and Planetary Science Letters, v. 317, pp.76-84, doi: 10.1016/j.epsl.2011.11.028.

Zhang, Y., Wallace, J.M. and Battisti, D.S., 1997, ENSO-like decade-to-century scale variability: 1900–93: J. Climate, v. 10, p.1520-0442.

Appendix A

Lithologic and Stable Isotope Stratigraphy of the Española Basin, NM
Note: This figure does not print well; see Supplement A for full resolution.

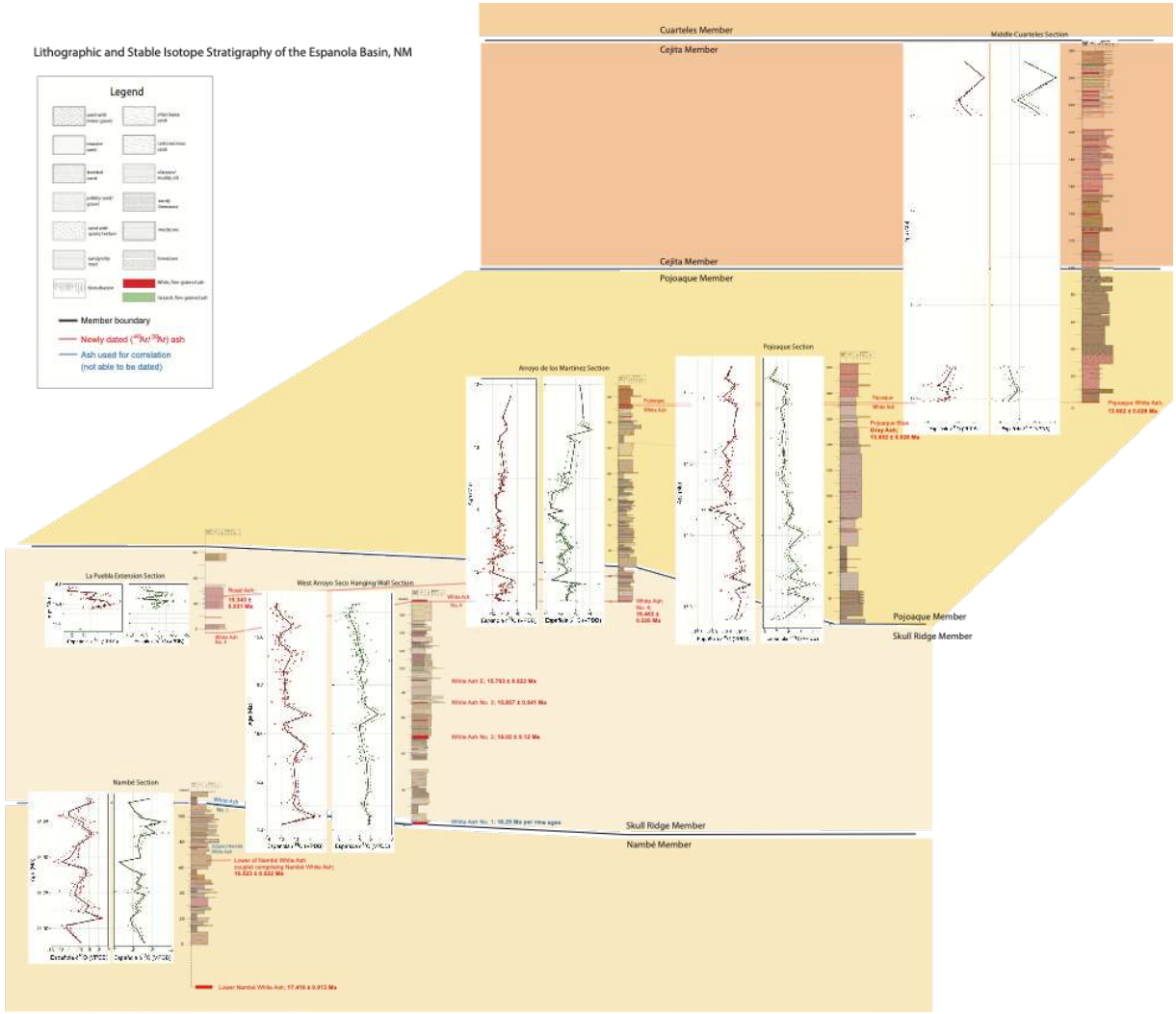

Appendix B

Details of Stable Isotope Laboratory Analyses

University of Wyoming Stable Isotope Facility carbonate $\delta^{18}O$ and $\delta^{13}C$ analysis

Principal of operation

The $^{13}C/^{12}C$ composition of carbonates is determined by acidification of the sample with 99.99% phosphoric acid. The method uses 12mL headspace vials as the vessel for acidification in conjunction with a gas chromatograph, which is coupled to an isotope ratio mass spectrometer in continuous flow mode. The head space vials containing the samples are flushed with helium. After flushing, 100µL of the phosphoric acid is injected into each vial. The samples are placed on the bench top at room temperature and allowed to react for 24 hours. After the reaction is complete, a sample of the headspace air is injected onto the gas chromatograph column for gas separation and isotopic analysis.

Gas Chromatograph conditions

Model	Thermo Gasbench
Column temperature	40°C
Column packing	Poraplot Q
Column length	30 meters
Column	13 psi

QA/QC

Quality assesment of carbon and oxygen isotope composition of carbonates is based on the standard uncertainty of the known value of the secondary laboratory reference material calculated on multiple analyses. For carbon isotope composition, if the standard uncertainty is greater than 0.15‰, the unknowns are re-analyzed (until the 2-sigma expanded standard uncertainty of the result is better than 0.3‰). The carbon isotopic composition is reported in per mil relative to VPDB scale such that NBS 18 calcite, NBS19 TS-limestone, and LSVEC lithium carbonate, respectively are -5.01‰, +1.95‰, and -46.6‰. For oxygen isotope ratio composition, if the standard uncertainty is greater than 0.2‰, the unknowns are re-analyzed (until the 2-sigma expanded standard uncertainty of the result is better than 0.4‰). The oxygen isotopic composition is reported in per mil relative to VPDB scale such that NBS 18 calcite, NBS19 TS-limestone, and LSVEC lithium carbonate, respectively are -23.2‰, -2.2‰, and -26.7‰.

There are 7 injections for each sample of which the last 6 are used to calculate an average. If the standard uncertainty of this average is greater than 0.5‰, the unknown is reanalyzed.

Normalization

Whenever isotopic analyses are performed, reference materials must be included with the unknowns. In general two 'bracketing' reference materials should be used for correcting purposes. These reference materials ideally would be similar in chemical complexity to the unknowns but have very different isotopic compositions. Using two such reference materials, you can generate two linear equations, one for each reference material. Since these linear equations will have the same slope and intercept, combining the two equations will generate a single linear equation that can be used to correct the unknowns.

The linear equation is derived as follows, where $\delta RM1 - known$ and $\delta RM2 - known$ are the accepted delta values of reference materials 1 and 2, respectively, and $\delta RM1 - measured$ and $\delta RM2 - measured$ are the measured delta values of the reference materials.

slope: $$m = \frac{[\delta\text{RM } 1 - \text{known} - \ \delta\text{RM } 2 - \text{known}]}{[\delta\text{RM } 1 - \text{measured} - \delta\text{RM } 2 - \text{measured}]}$$

intercept: $$b = \ \delta\text{RM } 1 - \text{known} - [\text{m} * \delta\text{RM } 1 - \text{measured}]$$

The normalization equation is as follows, where $\delta\text{SA} - \text{measured}$ and $\delta\text{SA} - \text{COR}$ are the measured and corrected delta values of the sample, respectively.

$$\delta\text{SA} - \text{COR} = \text{m} * \delta\text{SA} - \text{measured} + \text{b}$$

Colorado State University EcoCore Analytical Facility water $\delta^{18}O$ and δD analysis

Waters were analyzed on a Picarro L-2130i Water Isotope Analyzer coupled to a High Precision Vaporizer housed at the CSU Natural Resource Ecology Lab EcoCore Facility. Approximately 1.8 microliters were injected seven times; results are the average $\delta^{18}O$ and δD for the last four injections. Values of $\delta^{18}O$ and δD were corrected based upon measurements of USGS standards 45, 46, and 47. The analytical precision is better than 0.2‰ (2σ) for $\delta^{18}O$ and 0.5‰ (2σ) for δD.

University of Colorado Boulder Earth Systems Stable Isotope Lab $\delta^{18}O$ and $\delta^{13}C$ analysis

CUBES–SIL uses a Thermo Delta V gas source continuous-flow isotope ratio mass spectrometer. Samples are measured along with three to four standards that either have internationally accepted values or are in-house standards that have values determined relative to these standards (e.g., NBS-18, NBS-19, and LVSEC for light ^{13}C standards). Measurements of the standards bracket sample measurements in each run and are used to assess behaviors of the instrument that may need to be corrected. Standards covering the full range of signal intensities observed in the samples are measured to assess effects of linearity. Standards are also run intermittently throughout the analytical session to evaluate instrument drift over the course of a run. Lastly, the overall offset of the standards from accepted values is evaluated.

These corrections are done independently for carbon and oxygen and are checked using a monitoring standard that is treated as an unknown. In this dataset, linearity and drift were often negligible, and corrections for these effects were only applied when needed. Raw or linearity- and/or drift- corrected values were then corrected to final values similarly to UMSIL by applying a regression between two standards that span a range in values. Runs 1–13 and 15 used NBS-18 as the negative anchor for both $\delta^{13}C$ and $\delta^{18}O$, while runs 14, 16, and 17 used a MERCK carbonate as the negative $\delta^{13}C$ anchor point ($\delta^{13}C$ = -35.6‰) to better standardize for the range of $\delta^{13}C$ values found in typical terrestrial carbonates, following recommendations in Coplen et al. (2006).

Appendix C

Details of $^{40}Ar/^{39}Ar$ analysis
Provided by Matt Heizler

New Mexico Geochronology Research Laboratory $^{40}Ar/^{39}Ar$ analysis

The analytical data are organized to comply with FAIR (Findable, Accessible, Interoperable, Reproducible) data reporting norms of Schaen et al. (2020). The data are reported in an Excel workbook with data formatted within a variety of worksheets to facilitate ease of data viewing. Data are presented in isotope ratio and raw intensity format with the raw data sorted by sample name and laboratory run identifier. A summary data sheet is also provided the lists the preferred ages of the samples.

Sample separation included crushing and grinding if samples were highly cemented, otherwise pieces of the samples were placed in a blender and disaggregated in water. Samples where than treated with dilute HCl and HF (3 minutes) if necessary in an ultra-sonic bath. Following drying, the material was sized again using a typical 60-100 mesh fraction. This material was placed in heavy liquids to concentrate the K-feldspar fraction. Sanidine was selected by handpicking crystals while immersed in wintergreen oil using a polarizing transmitted light microscope. Following handpicking, crystals were thoroughly washing in acetone in an ultra-sonic bath.

Crystals were irradiated in three irradiations (see footnotes of ratio data worksheet) at either the TRIGA reactors in Denver, Colorado or at Oregon State University. Samples were typically placed in 1" diameter trays with 24 holes drilled around the perimeter. All irradiations included Fish Canyon Sanidine interlaboratory standard FC-2 in a known geometry to monitor neutron flux. In all cases FC-2 was loaded in the same trays as the unknowns and there are 8 locations within the 24-hole tray. Typically 8 grains from each monitor hole are analyzed and the J-value of the unknown locations is determined with a planar fit to the appropriate flux monitor locations. FC-2 is assigned an age of 28.201 Ma (Kuiper et al., 2008) and all ages are calculated with a ^{40}K decay constant of 5.463e-10 /a (Min et al., 2000). Isotope abundances are after Steiger and Jager (1977).

After irradiation, monitors and unknowns were loaded into stainless steel trays, evacuated and baked at temperature 100°C for 4 hours. A CO_2 laser was used to fuse the crystals. All samples were analyzed using an ARGUS VI multi-collector mass spectrometer equipped with five Faraday cups, and one electron multiplier (CDD) operated in ion-counting mode. The configuration had ^{40}Ar, ^{39}Ar, ^{38}Ar, ^{37}Ar and ^{36}Ar on the H1, Axial, L1, L2, and CDD detectors, respectively. Resistors were 10^{13} Ohms for ^{40}Ar and ^{39}Ar, 10^{14} Ohms for ^{38}Ar and ^{37}Ar and ^{36}AR was measured on the CDD. Extracted gas was typically cleaned with two NP 10 getters one operated at 1.6 A and one at room temperature. Some configurations utilized a cold GP-50 SAES getter as well. Gas cleanup times were typically 15-30 seconds that followed the 30-45 second fusion. The cleaned gas was expanded into the mass spectrometer for isotope analysis. All data collection was conducted with the in-house Pychron software and data reduction utilized MassSpec version 7.875.27A. Typically isotopes of low concentration samples were collected for 280 to 600 seconds followed by 60 to 180 seconds of baseline measurement. High concentration samples (large unknown grains and FC-2) were measured using 120 seconds of isotope collection followed by 30-60 seconds of baseline measurement. Analyses were truncated based on various criteria to facilitate efficient data collection. For instance, relatively old grains

that did not contribute significantly to age determination were analyzed for durations typically less than 60 seconds.

Extraction line blank behavior was relatively constant throughout this study owing to overall similar analytical protocols (blank values for each isotope analysis are given in the intensity worksheet). Following sample tray bakeout, ^{40}Ar and associated atmospheric ^{36}Ar were elevated and decreased throughout the course of data collection that typically took about 1-2 days to complete a sample run of 221 or 421 crystals. ^{40}Ar and ^{36}Ar blanks plus mass spectrometer background were typically 5e-17 and 4e-19 moles, respectively at the beginning of sample run. These values fell to about 2-3x less by the end of the sample run. In most cases large FC-2 grains were analyzed first because of low sensitivity to higher blanks and unknown sample grains were collected under lower blank conditions. To account for the time dependent blank behavior of ^{40}Ar and ^{36}Ar the blank data were typically fit as a time series commonly using a linear interpolation of bracketing blank intensities. Blank uncertainty for ^{40}Ar and ^{36}Ar was typically 2-5%. For ^{39}Ar, ^{38}Ar and ^{37}Ar the blanks are not time dependent and come mainly from the mass spectrometer backgrounds. Average values for ^{39}Ar, ^{38}Ar and ^{37}Ar blanks were at or below 1e-18 moles and typically had higher uncertainty of 10-50% related to detection limits of the Faraday collectors. Also during a data collection sequence, several air standards were run to monitor the $^{40}Ar/^{36}Ar$ detector intercalibration as well as a standard gas enriched in radiogenic ^{40}Ar and ^{39}Ar to monitor $^{40}Ar/^{39}Ar$ detector intercalibration. K-glass and CaF_2 were included in the irradiations to determine interfering reaction correction factors.

Choice of dates to define the preferred age is described in the manuscript. From these dates, a weighted mean age is derived from the inverse variance weighted mean (Taylor, 1982) and the error is the square root of the sum of $1/\sigma^2$ values. The error is also multiplied by the square root of the MSWD for MSWD greater than 1. J-error and irradiation correction factor uncertainties are included for all weighted mean errors that are reported at 2σ.

References

Kuiper, K. F., Deino A., Hilgen, F. J., Krijgsman, W., Renne, P. R., and Wijbrans, J. R., 2008, Synchronizing the rock clocks of Earth history. Science 320, 500–504.

Min, K., Mundil, R., Renne, P. R. and Ludwig, K. R., 2000, A test for systematic errors in $^{40}Ar/^{39}Ar$ geochronology through comparison with U–Pb analysis of a 1.1 Ga rhyolite. Geochim. Cosmochim. Acta 64, 73–98.

Schaen, A.J., Jicha, B.R., Hodges, K.V., Vermeesch, P., Stelten, M.E., Mercer, C.M., Phillips, D., Rivera, T.A., Jourdan, F., Matchan, E.L., Hemming, S.R., Morgan L.E., Kelley, S.P., Cassata, W.S., Heizler, M.T., Vasconcelos, P.M., Koppers, A.A.P., Mark, D.F., Niespolo, E.M., Sprain, C.J., Benowitz, J.A., Hames, W.E., Kuiper, K.F., Turrin, B.D., Renne, P.R., Ross, J., Nomade, S., Guillou, H., Laura E. Webb, L.E., Cohen, B.A., Calvert, A.T., Joyce, N., Morgan Ganderød, M., Wijbrans, J., Ishizuka, O., He, H., Ramirez, A., Pfänder, J.A., Lopez-Martínez, M., Huaning Qiu, H., Brad S. Singer, B.S., (in press), On the reporting and interpretation of $^{40}Ar/^{39}Ar$ geochronologic data, Geol. Soc. Am. Bull.

Steiger, R.H., and Jäger, E., 1977. Subcommission on geochronology: Convention on the use of decay constants in geo- and cosmochronology. Earth and Planet. Sci. Lett., v. 36, 359-362.

Taylor, J.R., 1982. An Introduction to Error Analysis: The Study of Uncertainties in Physical Measurements, Univ. Sci. Books, Mill Valley, Calif., 270 p.

Appendix D

Stratigraphic columns of the sections sampled in this study with tie lines correlating sections by common ash beds or lithologic features.